On the Seasonal Evolution of Thermophysical Properties and Passive Microwave Emissions from First-Year Sea Ice.

Isabelle Pacheco-Fernandes Harouche

A Thesis

Submitted to the Faculty of Graduate Studies

in Partial Fulfillment of the Requirements

for the Degree of

Master of Arts

Centre for Earth Observation Science

Department of Geography

University of Manitoba

Winnipeg, Manitoba

THE UNIVERSITY OF MANITOBA

FACULTY OF GRADUATE STUDIES

*****

COPYRIGHT PERMISSION PAGE

ON THE SEASONAL EVOLUTION OF THERMOPHYSICAL PROPERTIES AND PASSIVE MICROWAVE EMISSIONS FROM FIRST-YEAR SEA ICE

BY

Isabelle Pacheco-Fernandes Harouche

A Thesis/Practicum submitted to the Faculty of Graduate Studies of The University of Manitoba in partial fulfillment of the requirements of the degree of

MASTER OF ARTS

Abstract

The purpose of this study is to examine the utility of passive microwave emissions as a means of detecting the seasonal evolution of thermophysical changes in the sea ice observed through the period of winter to advanced melt. Brightness temperature (T_B) data were collected with a surface-based dual-polarized radiometer operating at frequencies of 19-, 37-, and 85 GHz. Both microwave emissions and thermophysical data were collected as part of the Collaborative-Interdisciplinary Cryospheric Experiment (C-ICE) between May 15 and June 25, 2000, in the Canadian High Arctic. Each stage was characterized by a running variance of the time series in the microwave emissions. The seasonal analysis was conducted taking into consideration observed changes in the physical characteristics of the sea-ice and the overlying snow pack. Results from a k-means clustering analysis show that variability in the microwave response can be categorized into phenomenological states earlier described by Yackel (2001) as *winter*, *ablation 1*, *ablation 2/3* and *ablation 4*. I describe the average thermophysical conditions associated with each one of these 'ablation states' and interpret the relative contributions of each to the observed microwave response. Emissivities were calculated and used as part of a descriptive analysis of the seasonal variation of T_B. The results confirm other findings that the strength and pattern of the relationship are frequency dependent and relative to snow and ice dielectric properties. Useful information on the thermodynamic state of the snow/sea ice system can be derived from passive microwave data since the microwave emissions respond to the general seasonal changes associated with the transition from winter to a melt-ponded sea ice surface.

Acknowledgements

This thesis would never have happened if it were not for the support, help, care and friendship of many people around me. I would like to extend my appreciation to my thesis advisor, Dr. David G. Barber for the opportunity of being part of such a significant endeavour as the C-ICE project and for all the suggestions that ultimately helped me steer this project to its final goal.

Thanks are due to all my C-ICE partners, for their help and presence both in the Arctic and in Manitoba. Special thanks go to Dr. John Yackel, C.J. Mundy, and John Iacozza, for their ideas, constant help and for introducing me to the mighty Canadian Arctic. I would also like to thank Carrie Breneman, Rob Kirk, Kim Morris, and Katherine Wilson for all the fun and learning during our field seasons, and David Mosscrop, Dr. Tim Papakyriakou, and Sheldon D. Drobot for their assistance at critical points in this thesis. I would like to acknowledge the staff at the Department of Geography, the Centre for Earth Observation Science and the University of Manitoba, in special Ms. Trudy Baureiss, Ms. Aggie Roberecki and Mr. Doug Fast for making my life a lot easier!

Sincere appreciation is extended to Mr. Ken Asmus, for so many things he taught me before, during and after both field seasons, for his attention, suggestions and insights, and to Dan Reimer for teaching me how to fly! A warm thank you to the staff at the Polar Continental Shelf Project in Resolute Bay, Nunavut; the warmest place in the Arctic. Thank you to Dr. Per Gloersen and Dr. Claire Parkinson at the NASA - Goddard Space Flight Center, for providing me valuable literature and some inspiring talks.

I would like to acknowledge the attention, care, and support of Lucio de Medeiros from the Electrical Engineering Department of the Catholic University of Rio de Janeiro, Brazil, who kindly took the time to help me in a rather complex point of this research.

In a more personal note, I would like to thank my mentor and friend, Dr. Dennis J. Murphy, from the Statistical Advisory Service at the University of Manitoba, for all our thought-provoking conversations and for teaching me that mathematics is the most exciting part of science. A very special thank you to Shawn Silverman, for proofreading this thesis, for his insights and for being such an endless source of inspiration. I also thank my friends Kitty Weg and Annie Goldberg-Eppinghaus for always being there and keeping my spirit up, even through e-mail!

Thank you so much to my friends from Washington, D.C, Carlos and Camilla, who have been helping my graduate career in more ways than they can imagine. Most of all, my work in Canada would not have been possible if it were not for the ongoing support of so many friends in the Winnipeg Jewish community. Thank you all, specially the Benamous, the Garlands, the Kellens, the Kogan-Gunns, and the Stelzers.

Last, but most definitely not least, I thank my parents, Edna and Paulo, for their love and support to this most eccentric daughter and for making sure that I could always count on them.

Table of Contents

List of Figures

List of Tables

List of Equations

CHAPTER 1 Introduction and Objectives

1.1 Introduction.

Sea ice represents an average of 10% of the total ocean cover on Earth (Parkinson, 1997) and it is an integral component of the polar climate system. The sea ice cap is the main element of the marine cryosphere, which, by means of feedback mechanisms, interacts with the overlaying snow cover, the atmosphere, and the underlying ocean forming the ocean-sea ice-atmosphere (OSA) interface[1] (Figure **1.1**). The total sea ice extent and thickness are key factors in the overall energy balance of polar regions (Maykut, 1978) and hence the marine cryosphere constitutes an important part of the global climate system (LeDrew, 1992).

The present concern with global climate change focuses attention on the marine cryosphere since it is considered to be a good early indicator of global climate variability and change (IPCC WG I, 2001 and Vinnikov *et al.*, 1999). Its rapid

---

[1] For the purpose of this research, except when describing specific snow volume or sea ice extent characteristics, snow and sea ice are seen as two parts of an integrated system, hereafter referred to as *snow-sea ice system*.

response to the presence of greenhouse gases in the atmosphere justifies the increasing interest in understanding the energy balances and exchanges at the OSA interface. The latest report published by the Intergovernmental Panel on Climate Change (IPCC) reveals that there has been a decrease in the summer sea ice extent of about 10 to 15% in the Northern Hemisphere since the 1950's. The same report states that a 40% decline in Arctic sea ice thickness in late summer and early fall and a gradual decline in winter ice thickness is presently observed (IPCC WG I, 2001).

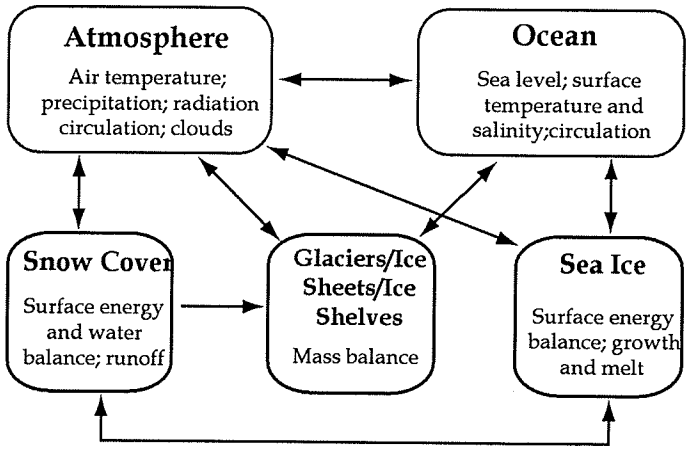

Figure 1.1. Diagram illustrating the interactions which take place in the marine cryosphere. The lists in the upper boxes indicate state variables and the lists in the lower boxes indicate processes involved in the interactions; arrows represent direct interactions (modified from Goodison *et al.* 1999).

In order to better understand and monitor the links between the snow-sea ice system and the rate and magnitude of climate variability and change, long-term observation and analysis of the polar physical environment are required. *In situ* data collection is an expensive and operationally complex activity due to a variety

of logistical challenges, such as vast spatial scales, difficult transportation, and hostile climate (Carsey *et al.*, 1992). The development and use of remote sensing tools for polar climate and cryosphere study is therefore a practical alternative for providing a broad area of fine spatial resolution observations. However, the use of remote sensors operating within the visible portion of the spectrum is impaired by the absence of solar light for approximately six months of the year and extensive cloud cover (particularly in the spring, summer and fall). This is not the case for both active and passive microwave sensors, which offer a powerful tool for obtaining large-scale geophysical data of remote, ice-covered oceans under all weather conditions irrespective of solar illumination (Onstott *et al.*, 1987 and Perovich *et al.*, 1998).

With the increasing demand for Arctic research (IPCC WG II, 2001) and the introduction of new sensors, there is a requirement for efforts in validation of passive microwave data of the snow-sea ice system in order to reduce uncertainties in the high-latitude climate simulations (Goodison *et al.*, 1999). The time series data now available from spaceborne platforms also call for understanding the relationship between passive microwave emissions and the thermodynamic and geophysical controls created by the seasonal transition from winter to summer in the Arctic (Barber *et al.* 1998 and Gogineni *et al.* 1992). The use of surface-based microwave radiometers, which collect high spatial and temporal resolution data from a fixed area, can be useful in understanding how spaceborne data at regional

and inter-annual time scales can be applied to climate research. The juxtaposition of the afore mentioned scales is useful for testing micro scale phenomena, which drive the snow-sea ice system seasonal evolution (Asmus and Harouche, 2000).

1.2 Research Design

My thesis is concerned with the analysis of first-year sea ice ablation stages using time series surface-based microwave radiometry data. The general goal is to develop a better understanding of the electromagnetic interactions (at microwave frequencies) with a seasonally variable first-year sea ice volume. It is hoped that this surface-based approach will aid in the development of algorithms required for airborne and spaceborne passive microwave sensors data assimilation.

1.2.1 Mission Statement

Science Objective: "To describe the seasonal evolution of smooth, fast, first-year sea ice using microwave radiometry and to assess the applicability of different microwave frequencies in characterizing sea ice seasonal ablation stages."

1.2.2 Objectives

In this thesis I examine two interrelated objectives as follows:

Objective 1. (*a*) To quantitatively and qualitatively describe the seasonal evolution of microwave emissions at 19-, 37- and 85 GHz V- and H polarizations, beginning with a cold snow pack and ending with complete melt pond surface flooding; and (*b*) to explore the statistical relationship between selected thermodynamic and geophysical variables controlling the microwave time series over seasonal periods described in (a).

Objective 2. To assess the utility of the three analyzed microwave frequencies (19-, 37-, and 85 GHz) at both polarizations (V- and H pol) and to define which of the six channels or combination of channels provide an optimal characterization of the snow-sea ice system ablation stages.

1.3 Thesis Structure Review

This thesis is subdivided into five chapters. The first chapter is a preamble to the science context in which this research was developed and it delineates the purpose and goals of this thesis. The second chapter presents a literature-based scientific background for marine cryosphere research and discusses the physical basis for sea ice remote sensing. In addition, a literature review of microwave interaction theory is presented as a framework for interpretation of the results.

In *Chapter 3*, the field site, data acquisition methods and calibration of the microwave radiometer data are discussed. A thorough description of several instruments used in the data collection is provided. In *Chapter 4*, I present results pertinent to both *objective 1* and *2*. I conclude in *Chapter 5* with a review of the most significant results pertaining to each of the stated objectives, and by making recommendations as to the logical evolution of this research.

CHAPTER 2 Review of Literature

2.1 Introduction – The Marine Cryosphere

The marine cryosphere is formed by the snow-covered sea ice, the liquid ocean underneath and the overlying atmosphere. The marine cryosphere is an important component of the climate system since it has a major effect on surface albedo (Budyko, 1969), which in turn affects and is affected by energy and momentum balances at the sea ice surface boundary (Barry *et al.*, 1993). These relationships are intensified by climatic events such as increased air temperature due to the presence of greenhouse gases in the atmosphere (Vinnikov *et al.*, 1999). Research done by Kattenburg (1996) using a general circulation model (GCM) showed that high latitude areas are especially vulnerable to climatic changes caused by greenhouse gases. Hence, of all climate system components, the marine cryosphere is the most susceptible to global climate variability and change. Based on this idea it is essential to further develop the understanding of both the Northern and Southern Hemisphere marine cryosphere.

The Northern Hemisphere has larger sea ice coverage than the Southern Hemisphere due to a predominance of ocean water above a latitude of 65°N (Duxbury and Duxbury, 1993). Since this research is focused on the Northern

Hemisphere marine cryosphere, a description of the geographical characteristics of the Arctic Ocean follows. The Arctic Ocean is 9.5×10^6 km^2 in area of which one third corresponds to shallow shelf seas of no more than 200m in depth (Barry *et al.*, 1993). Its surface is covered by variable extents of sea ice according to season. Maximum ice coverage occurs in March when 15.4×10^6 km^2 of the total ocean area is covered by sea ice. The minimum areal coverage (7.0×10^6 km^2) usually occurs in September (Parkinson *et al.*, 1999).

The existence of open water areas represent only about 2% of the total winter ice extent, but the heat flux contributed to the atmosphere from these iceless areas is 1 to 2 orders of magnitude larger than ice-covered areas (Maykut, 1978). Therefore the decrease in ice extent enables an increase in ocean energy loss through evaporation (Q_E) as well as larger sensible heat transfer by convection (Q_H) from the ocean surface to the atmosphere, as described by [2.1] following Oke (1987):

$$Q^* = Q_H + Q_E + \Delta Q_S + \Delta Q_A \quad [2.1]$$

A net radiation surplus (Q^*) increase is indirectly linked to a decline in surface albedo (section 2.2.3), since lower albedo values facilitate further sea ice melting and consequent reduction in ice extent. On an annual basis the heat storage (ΔQ_S) can be assumed negligible for large water bodies and ΔQ_A is the horizontal heat flux within the water volume. The control which sea ice exerts on the surface energy balance is the primary scientific issue of importance in climate variability and change studies. Through my research I intend to approach the use of passive

microwave remote sensing data to estimate the thermodynamic and geophysical states of the snow-covered sea ice (hereafter referred to as *thermophysical states*) and thus be able to infer various elements of the surface energy balance.

2.2 The Characteristics of the Snow-Sea Ice System

2.2.1 Introduction

Sea ice is a low-density, morphologically complex material consisting of three phases: (a) solid water in the form of ice crystals; (b) pockets of liquid solution of brine distributed within the ice volume; and (c) air pockets. Depending on the variation of its constituents, there is a significant variability in its physical state and structure (Perovich *et al.*, 1998). The sea ice cap floats on sea water with approximately 90% of its mass and volume below the level of the sea surface (Parkinson, 1997). Although sometimes exposed to the atmosphere, during most of the year a snow blanket of varying depths and densities covers the sea ice. The thermophysical significance of this blanket and its relevance to the sea ice cover will be discussed later in this section. For the purpose of this thesis I consider the snow and sea ice as a coupled system, which affects and is affected by mass and energy fluxes across their interface. Therefore all the analyses presented in this investigation were done considering the snow and sea ice volumes as a continuum, hereinafter referred to as the *snow-sea ice system.*

Among the climatic roles played by the snow-sea ice system, its insulating characteristic is the most important. In the winter, it isolates the warmer ocean underneath from the considerably colder atmosphere above. It also works as a solar radiation reflector and as a shield preventing mass, heat and momentum transfer between the ocean and the atmosphere (Barry, 1983). Hence the energy balance in the Arctic environment is directly dependent on the very existence of the snow-sea ice system itself. It is important to emphasize that Parkinson *et al.* (1999) have detected a negative trend in the Northern Hemisphere ice extent between 1978 and 1996 with an overall decrease of 34,000 ± 8300 km^2/yr. In addition to ice extent, ice concentration and open water distribution are yet other ways of determining the significance of the snow-sea ice system in the Arctic energy balance. Ice concentration is expressed in tenths per unit area (CIS, 2001). Concentrations close to marginal ice zones vary greatly with seasons but for the inner pack, summer concentrations vary between 85-95%, surpassing 97% during the winter (Gloersen *et al.*, 1992). Open water areas can occur year round in the form of leads (linear open water from 10-1000m wide) or larger non-linear areas known as polynyas. As mentioned in section 2.1, the open areas are responsible for a substantially larger heat input in the atmosphere when compared to ice covered areas.

2.2.2 The Geophysical Characteristics of the Snow-Sea Ice System

The World Meteorological Organization classifies sea ice according to varying developmental stages of the ice (relative to the time of formation), as well as thickness, salinity and roughness (WMO, 1970). The Arctic marine ice cover can be divided into two categories: first-year ice (FYI) which represents the new ice formed during a single year's winter (Figure 2.1) and multi-year ice (MYI) which has lasted one or more summer melts. In my thesis I deal only with first-year ice forms thus I will limit my review to the same.

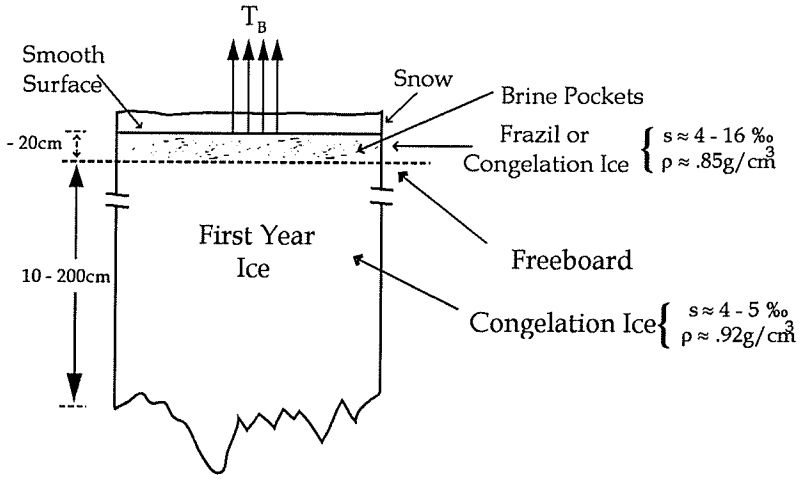

Figure 2.1. Schematic diagram illustrating the basic features which characterize the snow-sea ice system for a first-year sea ice volume (modified from Comiso, 1983).

First-year sea ice development is a consequence of the decrease in air temperature leading to temperatures below the freezing point on the wate surface, as well as the subsequent transfer of turbulent heat and loss of longwave radiation from the ocean surface to the atmosphere (Papakyriakou, 1999).

The exact temperature (in °C) for sea water to freeze varies relative to the amount of salt present [2.2], following Neumann and Pierson (1966):

$$T_f = -3\times10^{-3} - 5.27\times10^{-2} S_W - 4\times10^{-5} S_W{}^2 \qquad [2.2],$$

where T_f is the temperature of freezing and S_W is the sea water salinity in parts per thousand. The first stage in FYI growth is the formation of platelets and needle-shaped crystals referred to as *frazil* (Figure 2.2), which are most common under windy conditions (Barber *et al.*, 1994). With the increasing volume of frazil an incoherent mixture of unconsolidated crystals and sea water, known as *grease ice*, then develops. Continued freezing forms an elastic layer no thicker than 10cm called *nilas*. The continuing effect of wind and wave action can cause the formation of pancake ice consisting of quasi-circular masses created from semi-consolidated frazil.

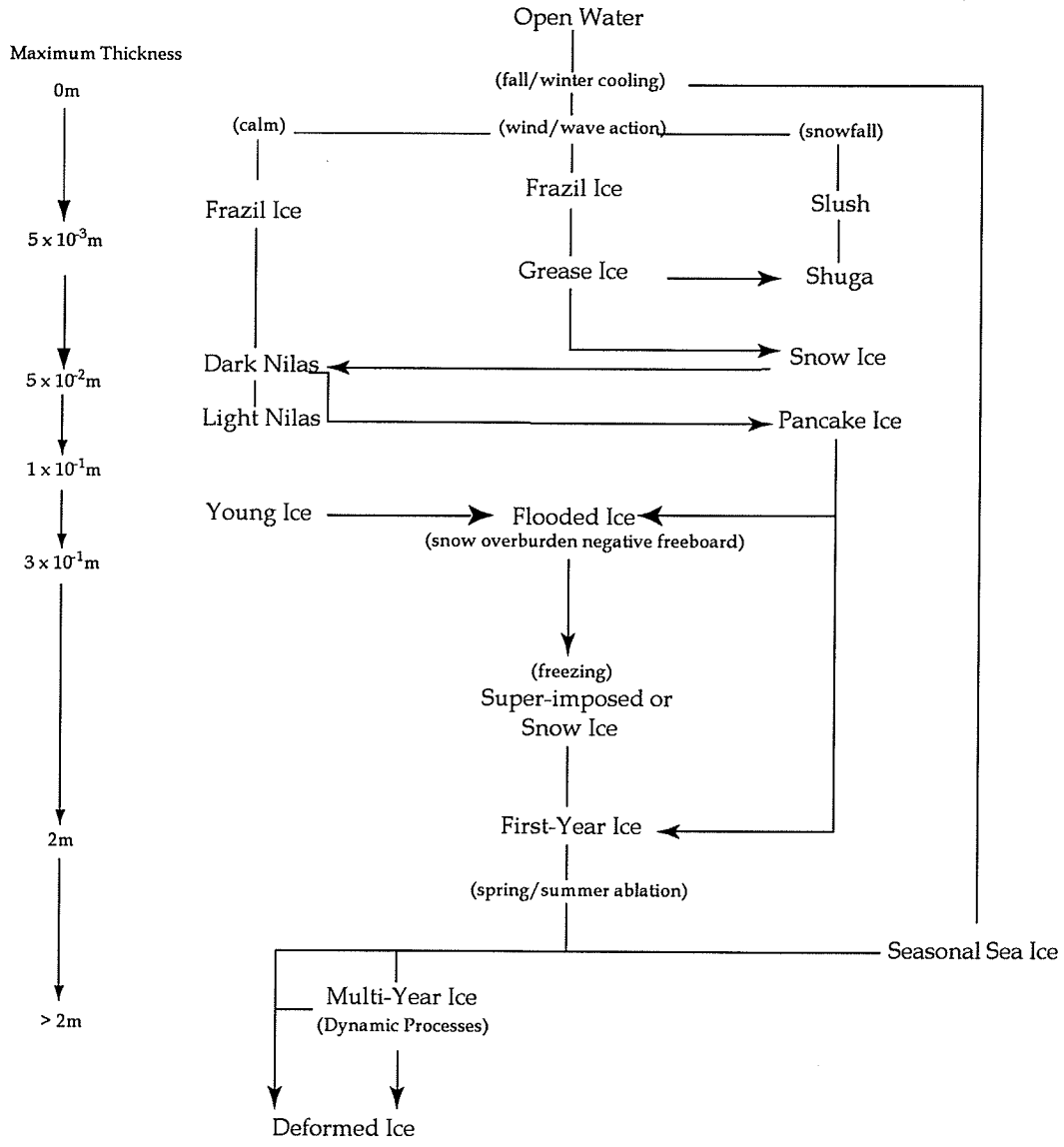

Figure 2.2. Chart with snow-sea ice system seasonal evolution stages. The environmental forces driving these stages is shown in brackets (adapted from Papakyriakou, 1999).

Once the temperature gradient between the frozen ocean surface and the overlying atmosphere decreases, ice growth-rate also decreases. At this point the ocean surface is already covered by a thin but consistent ice sheet, preventing further wind forcing under the ice cover. Additional ice formation occurs mainly at the bottom of the ice sheet. The FYI volume is then characterized as

having 3 texturally different layers, which thickness is a function of ice growth. Figure 2.3 shows the structure of a typical section of FYI: (a) dry snow layer with varying thickness usually averaging between 20 and 30cm (Iacozza and Barber, 1999); (b) randomly oriented frazil crystals overlaying (c) vertically oriented columnar ice grains. Columnar ice is formed under quiescent conditions (due to the nilas layer) and is distinguished by elongated crystals generally arranged according to the current motion vector present at the ice-water interface at the time when freezing occurred (Stander and Michel, 1989). Such crystals reach tens of centimeters in length and millimeters to a few centimeters in diameter (Tucker *et al.*, 1992). Each crystal has a substructure formed of ice plates spaced in tenths of millimeters by layers of brine inclusions. The volume and distribution of these brine inclusions are temperature related and associated with ice growth-rate, i.e. higher salinities are associated with colder temperatures and faster growth-rates (Weeks and Ackley, 1986 and Nakawo and Sinha, 1984).

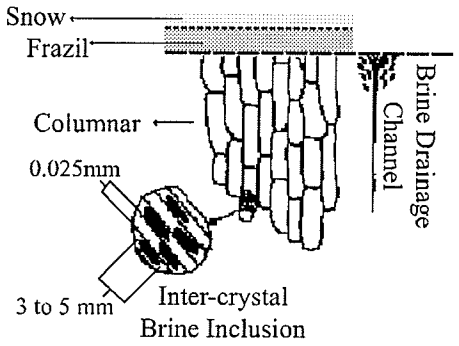

Figure 2.3. Schematic diagram illustrating a typical winter FYI section and later brine drainage channel (adapted from Vant *et al.*, 1978).

Once FYI is established, it generally has a smother surface than MYI, but the seasonal evolution of the snow-sea ice system will affect the surface roughness following mechanical and thermophysical processes (Swift *et al.*, 1992) as will be discussed in section 2.2.4.

It is worth noting that Rothrock and Thomas (1990) estimate that FYI accounts for 40% of the total Arctic Ocean cover and the seasonal variation of the total Arctic ice extent is primarily due to the inter-annual freeze-thaw cycles of FYI in marginal Arctic seas.

2.2.3 Energy Flux in the Snow-Sea Ice System

The surface energy balance is the leading phenomenon in the seasonal variation and decay processes in the snow-sea ice system (Zhang et al., 1996). It affects snow morphology and snow wetness, and consequently it changes the snow density (Barber, *et al.* 1995). However, physical changes observed in the sea ice volume do not react directly to variations in radiative and turbulent fluxes in the surface energy balance (Hanesiak *et al.*, 1999). Therefore in order to better understand the seasonal evolution of thermophysical and dielectric properties of the snow-sea ice system presented in 2.3.4 and 2.3.5, I introduce here basic concepts of energy fluxes in the snow-sea ice system. For the purpose of clarity, in what follows I deal with the snow-sea ice system as two interdependent parts: snow volume and sea ice volume.

The presence of an overlying snow volume with fluctuating thickness and density is of the utmost importance for the incoming energy propagation that actually reaches the sea ice surface, affecting its properties as a result (Barber et al. 1994; Brown and Cote, 1992). Whenever a sea ice sheet is present it serves as a depository platform for high albedo dry snow. Beneath the sea ice sheet, the underlying ocean is kept in a low-energy state since the turbulent heat exchange between ocean and atmosphere is constrained by the low thermal conductivity of sea ice (Nakamura and Oort, 1988). Garrity (1992) states that in order to understand the sea ice microwave emission properties (as presented in section 2.3) the overlying snow cover must also be studied.

Most of the energy balance and exchange taking place in the Arctic environment happens at the ocean-sea ice-atmosphere (OSA) interface. Considering that in most cases FYI is covered by snow, the radiative exchange at the snow surface follows [2.3] according to (Oke, 1987):

$$Q^* = K^* + L^* = K\downarrow - K\uparrow + L\downarrow - L\uparrow \qquad [2.3]$$

where Q^*, K^* and L^* are the net all-wave, net shortwave and net longwave radiative fluxes respectively; $\downarrow$ and $\uparrow$ represent incident and reflected energy. Seasonal evolution is defined by the changes in thermophysical properties of the OSA interface (Grenfell and Maykut, 1977), which in turn is partially determined by the incident shortwave radiation ($K\downarrow$) in the system (Maykut and Perovich, 1987) associated with an increase in atmospheric temperature. The change in

atmospheric temperature implies in a temperature gradient within the snow-sea ice system related to the conductive heat flux at the snow cover surface (Qc_0), sea ice surface (Qc_i) or at any depth inside the volume (Qc_z) according to [2.4], following Barber *et al.* (1994):

$$Qc_z = -\lambda_z \left(\frac{dT}{dz} \right)_z \qquad [2.4]$$

where λ is the thermal conductivity in watts per meter per degrees Celsius and $\left(dT/dz \right)_z$ represents the temperature gradient relative to depth. The redistribution of heat within the volume precedes melting, and hence precedes the existence of water in liquid phase.

The amount of $K\downarrow$ radiation emitted from the sun that actually reaches the snow-covered sea ice surface is a function of both the optical (Mellor, 1965) and thermophysical properties of the snow cover (Barber *et al.*, 1998) as discussed later in 2.2.4. Incident energy upon the snow-covered sea ice is reflected, transmitted or absorbed, but due to the high albedo of the snow cover, a considerable percentage of energy is reflected. Albedo (α) is the ratio of incoming radiation reflected from the surface according to:

$$\alpha = \frac{K\uparrow}{K\downarrow} \qquad [2.5].$$

The percentage of energy that is not reflected is then transmitted and partially absorbed through the snow volume. Since the snow cover has a higher shortwave extinction coefficient than sea ice, the amount of $K\downarrow$ reaching the ice volume is reduced at any level (z) at a rate approximately following Beers' Law [2.6]:

$$K\downarrow_z = K\downarrow_0 e^{-az} \qquad [2.6],$$

thus causing a delay in surface melt (Oke, 1987). With the onset of spring, the $K\downarrow$ input into sea ice becomes a function of the volume of snow or melt-ponds present on the ice (Grenfell and Perovich, 1984). Depending on the incidence of $K\downarrow$ into the snow-sea ice system, its physical characteristics will change, giving rise to diverse thermophysical evolution in the ice volume.

2.2.4 Thermophysical Characteristics of the Snow-Sea Ice System

Thermophysical properties are a function of the seasonal evolution of the temperature gradient between the atmosphere and the snow-sea ice system. These changes are defined as variations in the size and relative distribution of the snow-sea ice system constituent elements: brine, ice, and air. Figure 2.4 shows the relationship between the seasonal evolution experienced by these components as a function of changing temperature.

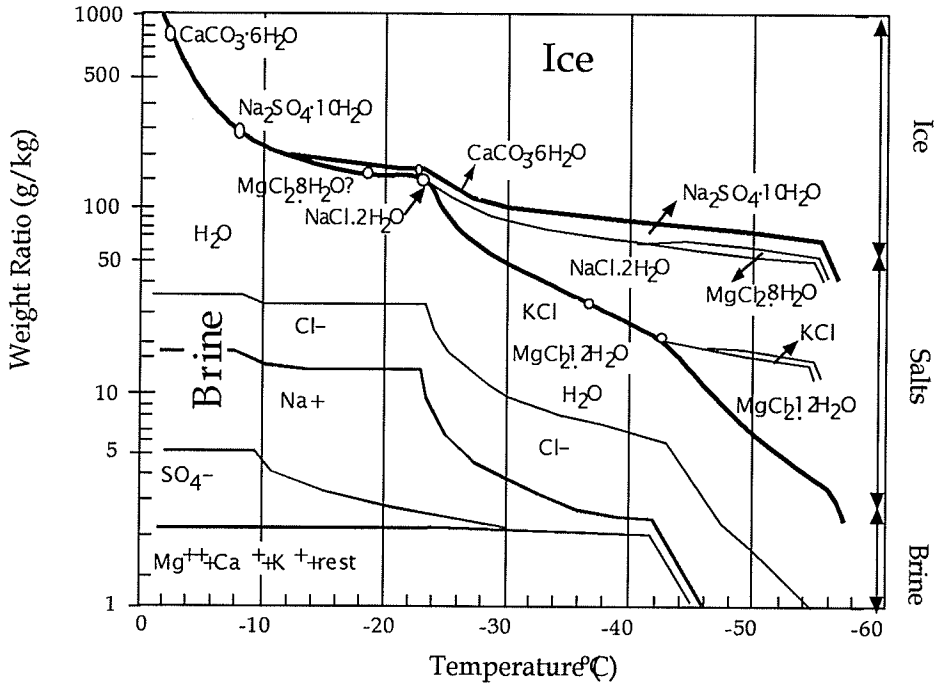

Figure 2.4. Diagram showing the phase evolution in the snow-sea ice system as a function of salinity and temperature and consequent changes in ice crystal, brine and solid salts (adapted from Weeks and Ackley, 1986).

Based on the thermophysical properties of sea ice, Livingstone *et al.* (1987a) classified five different sea ice "seasons". Later Yackel (2001) elaborated on a methodology for compartmentalizing the thermophysical evolution of landfast first-year sea ice, redefining the evolutionary stages into six *ablation stages*. In my thesis I deal with *winter* and *ablation stages 1* through *4*. A brief description of the physical characteristics of winter ice and subsequent ablation stages is presented below as a preamble to further discussion on microwave interactions during the snow-sea ice system decay season (presented in section 2.2.5). Both the Yackel (2001) and Livingstone *et al.* (1987a) nomenclatures are introduced

here for the purpose of comparison, but the remainder of my thesis will focus only on the Yackel (2001) nomenclature.

Figure 2.5 is presented as an illustration of the ablation stages as a function of incoming shortwave radiation ($K\downarrow$) and energy flux through the snow-sea ice volume.

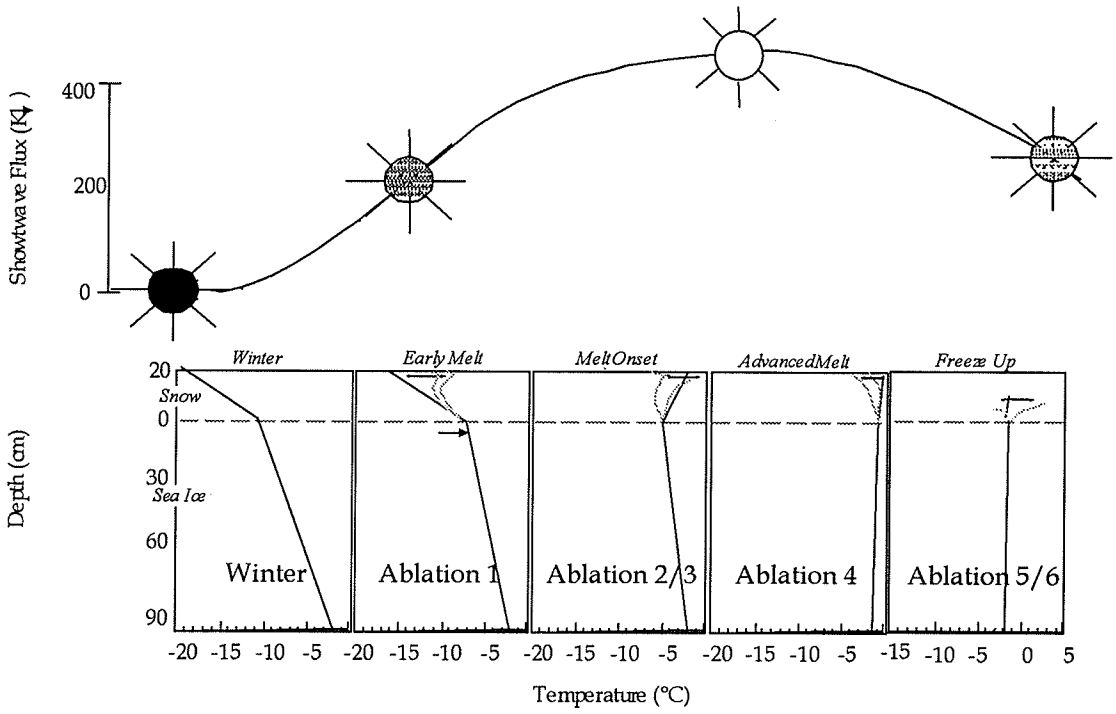

Figure 2.5. Simplified illustration for a 90cm deep ice pack representing the seasonal transition (from winter to ablation 5/6) of the thermodynamic regime present at the snow-sea ice system with shortwave influx description. The terms presented in italics correspond to the previously used descriptions of thermodynamic stages of sea ice according to Livingstone *et al.* (1987a). Modified from Barber and Yackel (1999).

Winter (*Winter*) – This stage is characterized by cold, dry ice with thickness varying from 30- to 200cm covered by a dry snow layer of varying depths. Ice density is uniform at 0.91-0.92 g/cm^{-3}. With increasing ice thickness the average

salinity declines (Eide and Martin, 1975), resulting in a "C"-shaped salinity curve with lower values in the mid-pack (4-5 ppt) and higher values at both extremes (5-16 ppt top, 30 ppt bottom) (Barber *et al.*, 1999). This pattern is a consequence of upward and downward brine expulsion during the freeze up period (preceding the winter) (Perovich and Gow, 1991), which tends to stabilize once the ice thickness reaches about 40 cm. During the winter stage liquid brine is found in ice grain interstitial space as well as elongated features named *brine channels*.

Cox and Weeks (1975) modeled sea ice salinity based on ice thickness according to equation [2.7] for ice thinner than 40 cm. This relationship explains 61% of salinity variation. Equation [2.8] accounts for 88% of salinity changes in cases where ice is thicker than 40cm.

$$S_1 = 14.24 - 19.39h_1 \quad [2.7]$$
$$S_2 = 7.88 - 1.59h_2 \quad [2.8]$$

In both equations, S is salinity in ‰, h_1 is ice thickness below 40cm and h_2 is ice thickness above 40cm. These conditions are usually observed from November to May. By the end of this period, the overlying snow temperature is such that the surface is warmer than the snow/ice interface by about 4°C (Garrity, 1992).

Ablation 1 (*Early Melt*) – This stage represents the transition from dry to wet snow (1% liquid water per volume) and the establishment of snow grain metamorphosis (Barber *et al.*, 1998) caused by daily air temperature oscillations and wind forcing. The ice sheet surface begins to roughen due to upward vapor mass transfer. Wind

forcing and frost flowers will also affect roughness (Swift *et al.*, 1992). Surface temperature can reach 0°C (273K). The enhancement in snow metamorphism may lead to either an increase or decrease in thermal conductivity of the snow pack. This in turn influences the length of time it takes for the surface temperature wave to propagate down to the ice surface determining the rate of change from solid to liquid phase at varying depths in the snow pack (Colbeck, 1982). At this point, ice lenses may be found within the snow volume (Garrity, 1992). In case snow precipitation takes place a new layer of low-density snow ($\approx 0.05 g \cdot cm^{-3}$) is deposited over an older, denser layer ($\approx 0.5 g \cdot cm^{-3}$) (Barber *et al.*, 1994), which causes a density gradient. During this stage, rapid changes in the geophysics of the snow are observed. This period ends when water in liquid phase is present throughout a diurnal period but surface ponds are not yet visible.

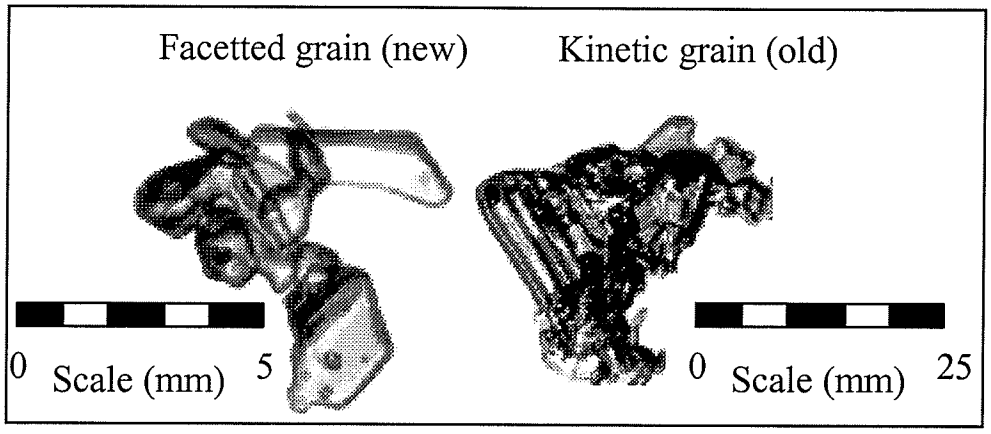

Figure 2.6. Morphological difference between a typical winter snow grain and a kinetic metamorphosed grain in the ablation 1 stage (adapted from Barber *et al.*, 1999).

Ablation 2/3 (*Melt Onset*) – In this stage, Yackel (2001) subdivided the melt onset regime into two distinct ablation stages based on snow grain morphological characteristics. Since a thorough analysis of snow morphology is beyond the scope of this research, both ablation stages 2 and 3 are merged into one for the purposes of this study.

At this point, the snow-sea ice interface is permanently damp, and water in liquid phase is present throughout the daily cycle at about 2% water per volume (Yackel, 2001), causing a decrease in surface albedo. More energy is conducted through the snow-sea ice system causing phase changes in the snow volume. Surface and subsurface freshwater ice layers develop as a result. Such phase changes will cause an increase in the volume of brine pockets. Increasing pockets will eventually interconnect, flushing the brine down and decreasing the ice's physical strength. Heat conduction models have been used to parameterize brine volume (Drinkwater and Crocker, 1988). A feedback mechanism is observed between thermal conductivity and distribution of brine pockets in that an increase in salinity inclusions will result in a reduction in thermal conductivity (Crocker, 1984). At this point, latent heat determines the thermodynamic interactions with the remaining snow cover and the melt ponds (Langham, 1981). The snow pack then becomes isothermal. In the event of snow precipitation and consequent increase in surface albedo, evolving snow-sea ice system conditions can still revert to winter conditions (Barber *et al.*, 1999).

Once water in liquid phase reaches about 7% water by volume the snow pack becomes saturated and drainage occurs. The drainage processes cause a liquid phase gradient in the snow patches with minimums at the surface and maximums in the basal layer, where large, metamorphosed grains ($\approx 70 - 100$mm) are found. In this stage, the snow-sea ice system has changed sufficiently to prevent any reverse to previous winter conditions. The recently formed brine channels are flooded with snow melt water, thus decreasing salinity in the snow-sea ice system. This stage ends with ponds starting to show and the presence of an extremely wet snow cover.

Ablation 4 (*Advanced Melt*) – The remaining snow cover is saturated throughout its volume. Remaining snow patches tend to melt completely as a result of stronger temperature gradients enabling kinetic grain growth (Barber *et al.* 1995). Once the melt ponds interconnect, drainage follows, forming a drainage basin flowing towards seal holes, cracks and leads. Conversely, melt ponds might increase in area and depth in case melting from surrounding snow is larger in volume than the drainage itself (Holt and Digby, 1985). Negative feedback is established between pond surface area and surface albedo, i.e. lower surface albedo enhances melting (Yackel *et al.*, 2000a). The snow-sea ice system undergoes cyclical surface melting and salinity decreases as the brine is being flushed to the ocean through interconnected brine channels (Vant *et al.* 1978). These channels are formed once brine volume exceeds 5% by volume and brine

pockets align parallel to adjacent columnar grains (Figure 2.3), eventually connecting. This season ends once snow patches have reduced in area and surface flooding is predominant.

2.2.5 Dielectric Properties of the Snow-Sea Ice System

Sea ice thermophysical characteristics vary greatly both in vertical and horizontal dimensions, and directly affect the propagation of electromagnetic waves in the sea ice volume. Hence, it is essential to understand the nature and magnitude of such changes in order to interpret microwave interaction in the sea ice.

The constituent elements of sea ice include freshwater ice, liquid brine and air, and to each element corresponds a characteristic relative dielectric constant (ε^*), a complex quantity indicated by:

$$\varepsilon^* = \varepsilon' - j\varepsilon'' \quad [2.9]$$

where ε' refers to the permittivity and ε'' refers to the loss of the material and $j = \sqrt{-1}$. Since the snow-sea ice system is a mixture of three different media, the complex dielectric constant of sea ice is an aggregate of the dielectric properties of each medium. From a physical perspective, ε^* is also affected by shape, size, and orientation of brine and air pockets relative to the electric field of the emitted wave, and also by their volume fraction and spatial distribution. The amalgamated medium combining all three parts vary through the seasons according to ice

temperature (Hallikainen and Winebrenner, 1992). Hoekstra and Cappillino (1971) defined a linear function associating the permittivity of sea ice (ε'_{si}) to volume fraction of brine inclusions (V_b) as:

$$\varepsilon'_{si} = \frac{\varepsilon'_i}{(1-3V_b)} \qquad [2.10],$$

where ε'_i is the permittivity of pure ice. Considering that FYI is usually covered by snow, the dielectric constant of the snow volume will ultimately influence the total energy emitted by the snow-sea ice system. It follows that the dielectric constant of dry snow (ε^*_{ds}) is governed by the dielectric properties of ice and also snow density (ρ_s). Note that since ε'_i is independent of temperature and emission frequency in the microwave region, then so is the dielectric constant of dry snow $\varepsilon*_{ds}$. Glen and Paren (1975) quantified $\varepsilon*_{ds}$ as:

$$\varepsilon'_{ds} = (1+0.47V_i)^3 = (1+0.51\rho_s)^3 \qquad [2.11],$$

where V_i is the ice-volume fraction related to snow and ice density:

$$V_i = \frac{\rho_s}{\rho_i} \qquad [2.12].$$

With the onset of the snow-sea ice system ablation (characterized by a minimal increase in liquid water available in the system), the complex dielectric constant of the snow-sea ice system radically changes. Knowing that the permittivity of water

is about 40 times larger than that of ice and air, the seasonal dielectric evolution of wet snow is a function of the volume of water present in the system.

The permittivity of wet snow (ε'_{ws}) is governed by frequency, temperature, water volume, snow density and the geometrical shape of both ice particles and water inclusions (Hallikainen and Weinebrenner, 1992). Work done by Hallikainen *et al.* (1986) shows a significant increase in ε'_{ws} relative to change in liquid water content in the snow-sea ice volume varying from 0- to 12% liquid water. The responses from both the 19- and 37 GHz channels frequently present increases in permittivity and loss due to increasing water volume content. However, the 37 GHz channel causes changes in a linear fashion with near-constant increments in ε* for different amounts of water available in the system. Responses from the 19 GHz channel have more variability and behave exponentially. The reader is referred to Hallikainen and Weinebrenner (1992) for a detailed account on the model describing the dielectric behavior of wet snow through the seasonal evolution.

2.3 Passive Microwave Interactions in the Snow-Sea Ice System

2.3.1 Introduction

Passive microwave radiometry has been used in sea ice research for over 30 years (Parkinson and Gloersen, 1993). Previous research has focused around three principles: (a) data from these sensors are sensitive to sea ice variability in both vertical and horizontal dimensions (Grenfell, 1986); (b) large expanses of remote areas impose several logistical challenges for *in situ* data collection; hence the need for data acquisition and monitoring from a distance; and (c) brightness temperature (T_B) data are retrieved by passive microwave sensors independently from sun illumination and cloud cover, which is virtually transparent in the microwave portion of the spectrum (Onstott *et al.*, 1987). The interpretation of T_B is based on two complementary aspects: (a) the seasonal evolution of the sea ice thermophysical properties (wetness, brine volume, density, grain metamorphosis) causes characteristic microwave emissions relative to observed frequency; and (b) the dependence on incidence angle (Fung, 1994 and Ulaby *et al.* 1986a). In the following subsections I address the physical basis for the assessment of sea ice seasonal evolution using passive microwave remote sensing.

2.3.2 Brightness Temperature and Emissivity

The passive microwave signal analysis described in this research is explained in terms of brightness temperature (T_B), (also known as *radiometric temperature*) for snow cover on thick, smooth, first-year sea ice. Brightness temperature is a measurement relative to a *blackbody* (ideal emitter) radiating the same amount of energy per unit area as the observed body at the wavelength under consideration. The physical basis of T_B can be numerically described as [2.13] following Fung and Ulaby (1983):

$$T_B(\theta,\phi;i) = \frac{1}{L_a(\theta)}\left[T_{BS}(\theta,\phi;i) + T_{SC}(\theta,\phi;i)\right] + T_U(\theta) \qquad [2.13]$$

where T_B is the brightness temperature of the scene for a given solid angle (θ,ϕ) at polarization i (vertical or horizontal); and $L_a(\theta)$ is the atmospheric loss between the observed surface and the radiometer antenna. T_{BS} is the brightness temperature of the ground surface and T_{SC} is the scattered brightness temperature; T_U represents the upward brightness temperature of the atmosphere layer between the surface and antenna. In this research I make the simplifying assumption that a clear sky is always radiometrically cold and therefore free from water vapor. Hence the atmospheric loss can be discarded and both T_{SC} and T_U are set to zero.

It follows that the observed T_B has a direct relationship with emitted brightness temperature (T_{BS}) according to:

$$T_B(\theta,\phi;i) = T_{BS}(\theta,\phi;i) \qquad [2.14]$$

which is a function of the ground medium physical temperature according to:

$$T_B(\theta,\phi;i) = e_i(\theta,\phi)T_{phy} \qquad [2.15]$$

The emissivity $e_i(\theta,\phi;i)$ of a given media is described as the ratio of the radiant flux from the media per unit wavelength to that of a blackbody at the same physical temperature (Ulaby *et al.* 1986a). Emissivity is related to surface reflectivity (Γ) by:

$$e = 1 - \Gamma \qquad [2.16],$$

where Γ is the Fresnel reflectivity coefficient, which accounts for the dielectric mismatch between different media. In an ideal thermal-equilibrium condition, the energy absorbed must equal the energy emitted, hence maintaining the temperature distribution. Thus, the Fresnel reflectivity coefficient is a measure of the efficiency of a surface in reflecting electromagnetic radiation; it relates medium properties and geometry to measured power reflected from an interface.

It is governed by scattering properties of the surface and T_{phy} represents the physical temperature of the observed medium (Fung and Ulaby, 1983). Both T_B and T_{phy} are represented in degrees Kelvin.

2.3.3 Microwave Emission Properties of the Snow-Sea Ice System

Microwave emission is controlled by the evolution of thermophysical and electrical properties of the snow-sea ice system induced by seasonal changes. Therefore analyzing the temporal variations of microwave emissions can be used as a proxy to infer states in the sea ice decay process (Drobot and Barber, 1998). In what follows I examine a combination of factors influencing microwave emissivities from the snow-sea ice system, including: snow cover characteristics, ice surface roughness, brine volume, ice density, and ice thickness.

A characteristic microwave signature particular to each frequency corresponds to each stage of the seasonal transformation of the snow-sea ice system (Tjuatja *et al.*, 1993). This is due to the fact that the composition of the ice changes through the seasons and such composition determines the electrical properties of the media, which in turn defines the microwave emission characteristics. Figure 2.7 shows a schematic description of emissions at different frequencies relative to the seasonal evolution. The depth from which the bulk of emissions emanate is known as *optical depth*. For first-year ice, the optical depth is of the same order of magnitude as the wavelength of each frequency (Gloersen *et al.*, 1973). Table 2.1 shows the wavelength for the three different frequencies (Parkinson and Gloersen, 1993) analyzed in this research.

Table 2.1. Wavelength for observed frequencies.

Frequency	19 GHz	37 GHz	85 GHz
Wavelength	1.55 cm	0.81 cm	0.35 cm

In cases of snow-covered sea ice, the optical thickness is mainly determined by the free water distribution in the snow volume rather than the snow depth (Livingstone *et al.*, 1987b). In the presence of dry snow cover T_B readings were found to be independent of frequency and approximately equal to the physical temperature of the sea ice surface (Garrity, 1991).

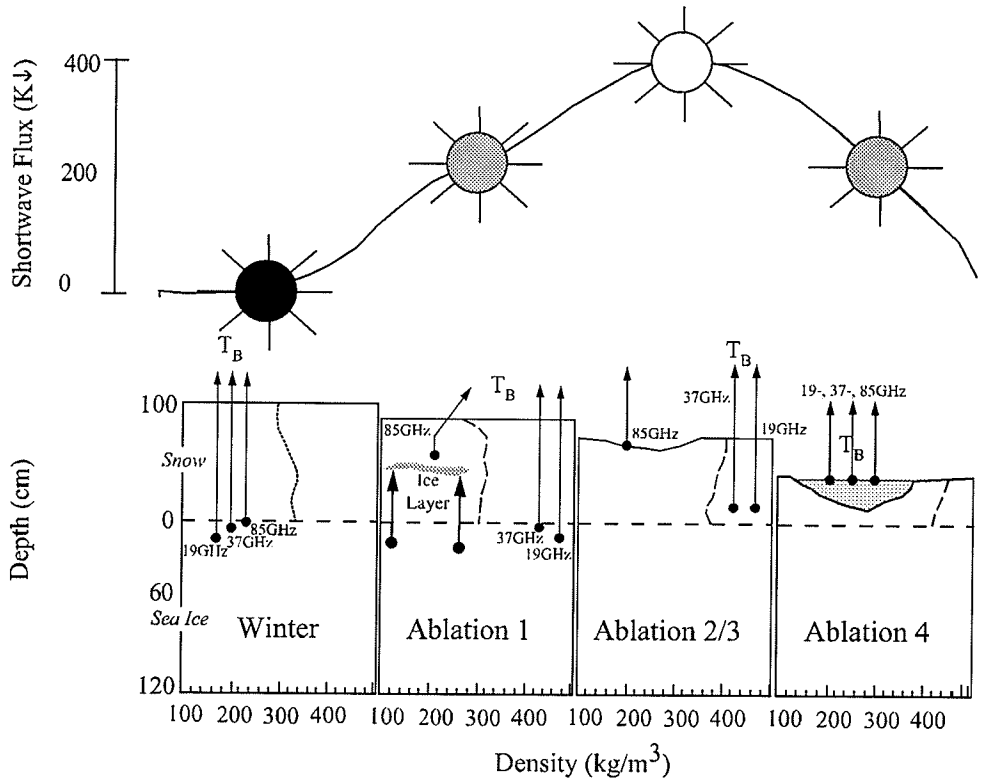

Figure 2.7. Schematic description of the seasonal evolution of microwave emissions relative to the depth of radiance. The dashed lines represent snow density profiles for each ablation stage.

Previous studies carried out by Livingstone *et al.* (1987a), Onstott *et al.* (1987), and Grenfell and Lohanick (1985) have shown that microwave emissions are

correlated with the volumetric proportions of water in liquid phase, and the amount of liquid brine and air (Tucker *et al.*, 1992). Furthermore, the thermophysical influence of sea ice on its microwave emissions is a function of frequency and depth in the ice volume where the emissions are being generated (Fung, 1994). It is believed that snow wetness as low as 1% is enough to sharply increase T_B (Mätzler *et al.*, 1982).

Salinity and ice layers at the snow-sea ice interface can significantly affect microwave properties of snow, causing the snow to mask the signature of underlying ice at frequencies where snow is optically thin (Drinkwater and Crocker, 1988). Upward brine expulsion, as a function of rising pressure inside brine pockets due to ice formation, produce a layer of highly concentrated brine at the snow-sea ice interface, which in turn contributes to the formation of a slush layer. Increase in brine as a percentage of snow volume contributes to a significant rise in T_B especially at 19- and 37 GHz. But often the slush layer refreezes causing decrease in emissions from frequencies below 40 GHz (Lohanick, 1990). This decrease is understandable especially when considering a potential ice obstacle to lower level emissions. With the onset of melt, the liquid water content present in the snow-sea ice system increases, consequently increasing surface reflectivity, since $e = 1 - \Gamma$. It then follows that T_B experiences a sharp decrease in emissivities at 19- and 37 GHz. Frequencies higher than

40 GHz do not show much change in absolute values of T_B since emissions are characteristically originated close to or at the skin surface.

Emissions are also affected by sea ice surface roughness. In general consolidated, landfast first-year ice consists of a smooth surface. First-year sea ice has been extensively studied in the Canadian Archipelago, where data collection for this research was performed (e.g. Yackel *et al.*, 2000b; Barber and Yackel, 1999; Drobot and Barber, 1998; and Grenfell and Lohanick, 1985). In this area, landfast sea ice is smoother and undergoes less mechanical surface deformation than on more wind-exposed areas such as the Beaufort Sea and Labrador Sea (Paterson *et al.*, 1991).

2.3.3.1 The Role of Frequency and Polarization in Microwave Remote Sensing of the Snow-Sea Ice System Ablation States

The analysis of different frequency and polarization combinations allows us to extract more information from the microwave emissions of the seasonally evolving snow-sea ice system. In general, frequencies provide us with different sensitivities to the brine and phase relationships as they change throughout the season. Lower frequencies (longer wavelengths) originate lower into the snow-sea ice system and thus are not as sensitive to atmospheric driven changes in brine volume and or phase changes. Higher frequencies (shorter wavelengths) originate higher up in the system, close to the boundary between snow-sea ice system and atmosphere, and are, in general, more sensitive to atmospherically forced changes

in the thermophysical properties of the system. Polarization provides differences which can be attributed to the physical structure of the snow-sea ice system (Ulaby *et al.*, 1986a). Shifts in signature from different polarizations are specially useful at providing information regarding the nature and properties of surface and volume microwave emissions. Brightness temperature curves at both V- and H polarizations tend to increase with rising surface roughness. Ulaby et al., (1986b) pointed out that as roughness height increases from 0.88cm to 4.3cm, the emissivities approach polarization independence.

The scientific literature reflects the fact that very little high temporal/spatial resolution data exist over the full time period from winter to summer for snow-covered sea ice. Most of the past work has been based upon satellite systems, which have very coarse spatial resolution or from time series surface observations with a limited temporal resolution.

Within the approximate 9-month period comprising fall, winter and most of the spring, microwave emissions from sea ice have been analyzed over a broad range of frequencies (e.g. Grenfell *et al.* 1998; Jezek *et al.* 1998; Tucker *et al.* 1991; Hollinger *et al.* 1984; Troy *et al.*, 1981). At this point the responses gathered from different frequencies have minimum diurnal variation (Livingstone *et al.* 1987b), with standard deviation of 3% (Comiso, 1983). The signatures from 19- and 37 GHz are quite similar at times with a difference of less than 2 K. Lomax *et al.* (1995) stated that 85 GHz signatures are very much like lower frequencies in

terms of daily variance with slightly lower absolute T_B values. With the onset of melt and the increase in volume of liquid water available in the sea ice system, emissivities from different frequencies change in a non-linear fashion with noticeable differences among frequencies (e.g. Lubin *et al.*, 1997; Comiso and Kwok, 1996; Onstott *et al.*, 1987; Carsey, 1985).

Emissivities at vertical polarization decrease at 37 GHz responding to presence of water in liquid phase. Frequencies Lower than 37 GHz have a greater drop whereas higher frequencies experience a lower decrease or even some increase in emissions when compared to the fall/winter months. The H pol response to the onset of melt is very similar to V-pol only with higher amplitudes during the summer months and lower absolute values throughout the year. Generally when dry snow is present the spacing between polarized T_B tends towards a minimum. For better interpretation of snow cover effects, the comparison between both polarizations of a same frequency yields better results than comparisons of different frequencies at the same polarization (Comiso, 1985).

During the melt onset period, ice lenses within the snow pack are observed as an outcome of freeze-thaw cycles. These ice lenses together with new dry snow accumulation following sporadic storms cause a decrease in horizontal T_B for frequencies between 5- and 35 GHz. Measurements from 85 GHz are not affected by the presence of mid-snow pack ice lenses due to its shallower optical depth (Garrity, 1992).

Livingstone *et al.* (1987b) showed that at higher incidence angles the emissivity standard deviation was larger (19 K) than for lower incidence angles (5 K) for both dry and wet snow-sea ice volumes. However, when comparing between dry and wet volumes, results from lower incidence angles had larger differences (up to 3 K) among themselves.

In research done with frequencies of 10-, 18-, 37-, and 90 GHz, Grenfell (1986) presented results where 90 GHz had less summer variation than lower frequencies. This was attributed do the fact that, at lower frequencies, emitted radiation comes from deeper in the ice column (see Figure 2.7) and is more sensitive to subsurface ice structure.

2.4 Summary

This chapter has introduced the integrated snow-sea ice system as the main component of the marine cryosphere. A comprehensive description of thermophysical and dielectric characteristics of the system was presented in the context of seasonal evolution. The seasonal transitions were described as a function of feedback mechanisms occurring in the ocean-sea ice-atmosphere interface, which in turn are triggered by the energy flux observed in the system. The characterization of the snow-sea ice system was used as a premise to describe microwave emissions' seasonal evolution, defined as a proxy in the assessment of seasonal characterization of the snow-sea ice system itself.

Together with the research objectives stated in *Chapter 1*, the information presented in this chapter will serve as the basis for the data analysis and the discussion of results presented in the following chapters.

CHAPTER 3 Data Collection and Analysis Methods

3.1 C-ICE 2000 Campaign

Data used in this research were collected in 2000 during the Collaborative-Interdisciplinary Cryosphere Experiment (C-ICE). C-ICE is a longitudinal field experiment conducted annually during spring and/or summer months in areas adjacent to Cornwallis Island in the Canadian Archipelago. The C-ICE 2000 campaign took place both on and near Truro Island (75°14.623'N, 97°09.566'W) (Figure 3.1). Data collection started on the last week of May (Year Day – YD 136, May 15 – please refer to Appendix A), and were done over consolidated, landfast, snow-covered, thick first-year sea ice. The sampling site was located in McDougall Sound, 2 kilometers east of the island. The area was characterized by smooth first-year sea ice approximately 150cm thick at the beginning of the field season. Snow depth ranged from 8 to 18 cm in the vicinity of the study area. The collection period extended until June 26 (YD 177), when the ice was still landfast, but with no significant snow cover left. In some areas total surface flooding was observed. All measurements were made based on local Central Standard Time (CST).

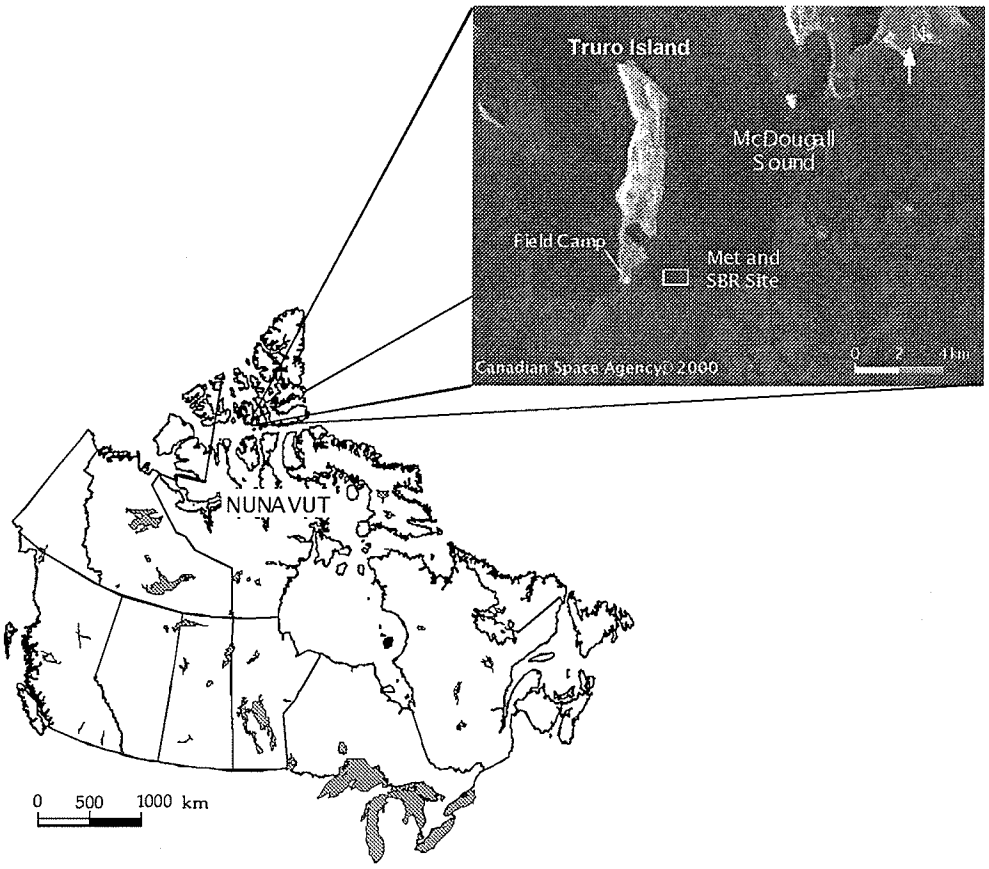

Figure 3.1. C-ICE 2000 field location. Insert illustrates field configuration and SBR platform position relative to the main camp.

3.2 Surface-Based Radiometer

3.2.1 Introduction

Time series from satellite-based passive microwave sensors have recently been examined to define different stages in the snow-sea ice system decay and extent (Parkinson *et al.* 1999; Comiso and Kwok, 1996; Gloersen *et al.*, 1992). Grenfell *et al.* (1998), Tucker *et al.* (1991) and Livingstone *et al.* (1987b) made detailed descriptions of specific ice stages using data from discrete points in time. In each of these studies the data were obtained either from marginal ice zones or regional

estimates of a mixture of ice types. In this research, the analysis of transitional periods over landfast first-year sea ice is focused at one fixed geographical location as a means of testing the microwave interaction theory from a microscale perspective, as well as simplifying the relationship between ice type, microwave emission and the seasonal evolution of these covariates.

This experiment made use of a unique microwave radiometry data set collected in the course of 40 consecutive days at the same location. The surface-based radiometer used for this sampling program was a dual-polarized system operating at the frequencies of 19-, 37-, and 85 GHz, with the antennas deployed at a 53°-incidence angle. The choice of frequencies and incidence angle was done with the aim of mimicking the pre-existing Special Sensor Microwave/Imager (SSM/I) spaceborne sensor on board of the American Defense Meteorological Satellite Program (DMSP) platform. The radiometry data present a comprehensive time series of the evolution of microwave emissions from the snow-sea ice system and it is described in terms of brightness temperature (T_B).

The surface-based radiometer (SBR) was deployed on a ground-mounted fixed configuration at 3.5m above the ice surface (Figure 3.2). The SBR used 15° beamwidth antennas, with one for each frequency. Considering both incidence angle and distance from the surface, the field of view presented the following parameters: 1.31m near width, 1.87m far width, and 2.62m in depth.

Figure 3.2. SBR system at fixed deployment site.

The system was connected to a computer-controlled positioning platform for controlling azimuth and elevation. Due to a unit failure, the positioning was done manually with the use of an analog protractor levelled perpendicular to the axis along to which the antenna was pointing. Data was stored in a data acquisition computer containing the SBR software. Measurements were acquired in voltages and, through a software model, converted to surface radiance expressed in T_B (please refer to section 2.3.2).

Two data collection modes were used for the microwave program. For approximately 23 hours a day the SBR would remain static, pointing down to the snow-sea ice system at an incidence angle of 53° from nadir. The control software

output 15-minute averages of microwave emissions captured by the sensors at a data-sampling interval of 68 seconds. This measurement routine was known as the *time series data collection*. An incidence angle *replicate sampling collection* was performed daily near solar noon. This procedure consisted of interrupting the regular data collection, moving the antennas to an incidence angle of 35° from nadir and activating the data retrieval controls in order to record 5 microwave emission readings. After these 5 replicates were collected, the antennas were moved consecutively in 5° increments between 30° and 70°, in total collecting five replicates from eight angles. Following the replicate sampling collection, the antennas were relocated at their original 53° position and the time series collection was then resumed. Further details on the daily operation of the SBR system can be found elsewhere (Asmus and Harouche, 2000).

3.2.2 System Calibration

A radiometer is considered calibrated once an accurate correspondence has been established between the receiver output voltage and the integrated absolute radiance captured by the antenna. The SBR system required calibration in order to accurately depict the surface radiance with minimum acquisition error. When accurate, the reference temperatures used in the calibration spans the range of observable T_B and 2 constants are determined, which in turn are used in the radiometer equation enabling the calculation of the calibration curve (please refer to Appendix E). A detailed description of the procedure for obtaining the

calibration curve can be found in Han and Westwater (2000). Due to logistical problems during data acquisition, several sources of potential calibration error were identified: radiometer pointing error, uncertainty in terms of water vapour present in the air, system random noise, and uncertainties relative to the measurement of blackbody temperature. For this reason the results presented in *Chapter 4* were analysed based on a relative calibration derived from the replicate sampling collection. In what follows I will discuss both the absolute and relative calibration procedures performed in this research.

The absolute calibration was performed whenever clear sky conditions were present following the tipping calibration method described in Han and Westwater (2000). It consisted of interrupting the time series collection and repositioning the antennas at a nadir-looking angle. At this point an Eccosorb© "hot load" (blackbody) at ambient air temperature was placed underneath the antennas. The SBR system would retrieve 5 microwave-emission replicates averaged over 68 seconds. The antennas were then moved to 120° pointing at the sky followed by consecutive 10°-increment angles up to 180° (zenith look) with the purpose of collecting a reference "cold load" temperature relative to the sky. Based on the data collected, the software calculated the sky's T_B and produced a new calibration equation to be used in all subsequent SBR measurements until the next calibration took place. There were a total of 7 calibration procedures

performed during the whole experiment period, which for the purpose of absolute T_B accuracy, was considered a low number.

The time series data used in this work relied upon the replicate profile measurements as a means of relative calibration. Each replicate scan was tested with a non-parametric Kruskal-Wallis test with 99% confidence level to ensure that each replicate scan could be considered as statistically equivalent. This test gave the assurance that the SBR was properly relatively calibrated over a 24-hour period. Figure 3.3 shows the time series evolution of the replicate means at each incidence angle. The error bars denote the standard deviation of the replicates representing a minute variance (less than 3%) among replicates, which means the sensors were sound and acquiring consistent data. The seasonal variability observed in the data is the basis for the relative calibration concept, in that the noise was much smaller than the seasonal variability. As expected, the 85 GHz channel presented more noise than the other two channels.

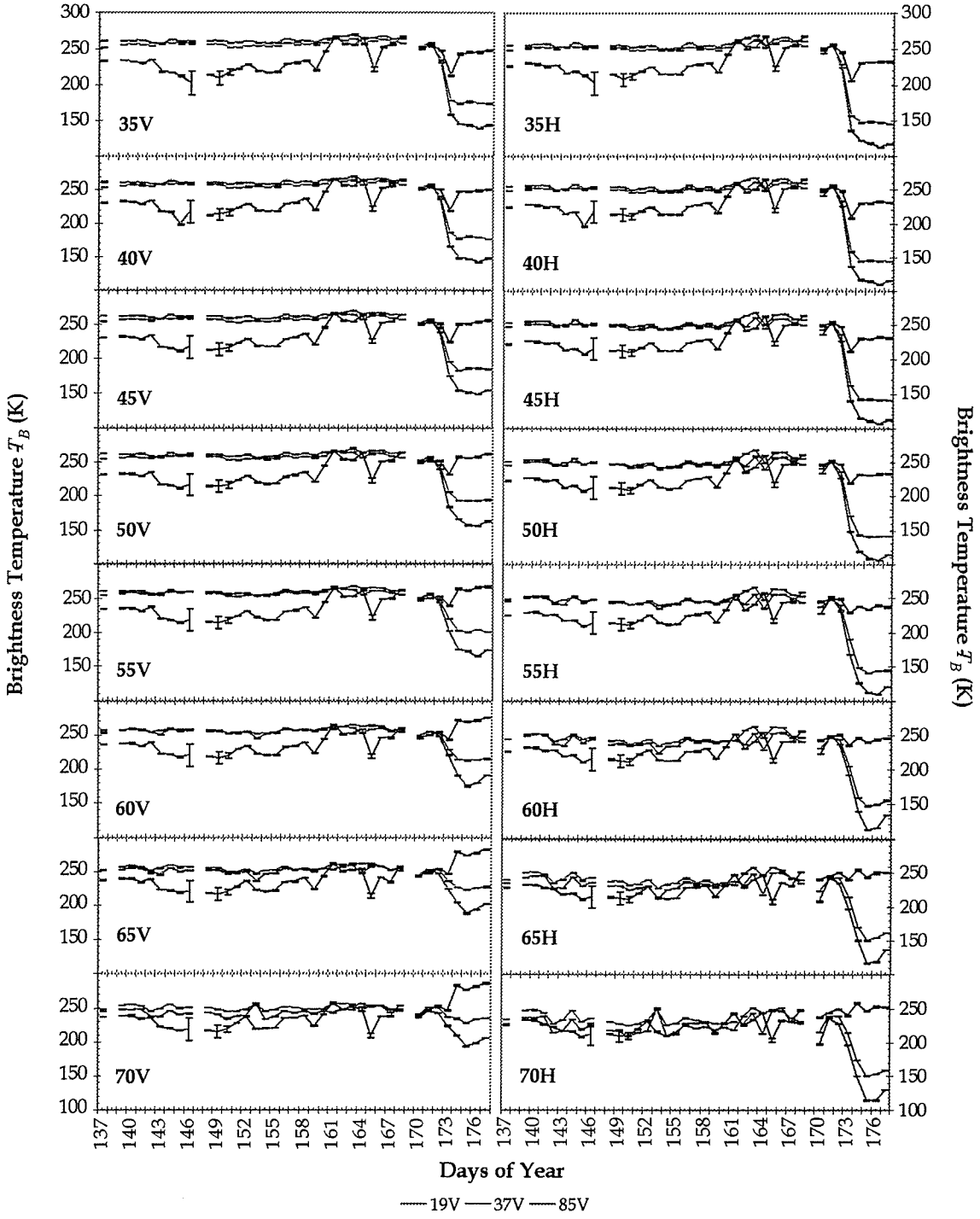

Figure 3.3. Time series of replicate sampling collection. The error bars denote the standard deviation among replicates.

Table 3.1 shows the T_B means and standard deviation for each season relative to each channel. This information was useful in determining if the difference

between V- and H pol was as predicted and the variability within each season indeed corresponded to what has been previously stated in the literature (Grenfell, 1986), confirming the validity of the relative calibration.

Table 3.1. Means and standard deviations for T_B collected at 53° incidence angle.

	19V	19H	37V	37H	85V	85H
Winter	247.57 ± 1.91	232.52 ± 3.86	247.35 ± 2.07	232.45 ± 3.05	222.40 ± 8.48	216.26 ± 7.35
Ablation 1	258.83 ± 3.66	247.36 ± 8.13	257.00 ± 4.68	247.44 ± 10.89	220.58 ± 22.88	217.11 ± 21.77
Ablation 2/3	261.52 ± 24.66	250.93 ± 34.65	258.44 ± 17.65	243.12 ± 26.10	230.03 ± 33.31	219.52 ± 31.37
Ablation 4	242.47 ± 4.36	228.50 ± 5.68	236.37 ± 2.10	221.44 ± 3.37	211.61 ±5.10	206.87 ± 6.55
Total	162.34 ± 28.41	110.84 ± 40.06	198.67 ± 18.99	144.44 ± 30.78	263.60 ± 23.49	238.38 ± 20.02

3.3 Thermophysical Data

Ancillary data were collected in order to characterize the thermophysical properties of the snow-sea ice system within and between seasonal evolution stages. The variables of interest in this experiment are the following: (a) sea ice physical temperature recorded at different depths from the ice surface; (b) snow cover physical temperature recorded at different heights from the ice surface; (c) snow cover salinity; (d) air temperature; (e) percentage of total sky cloud coverage; (f) qualitative snow grain description; and (g) sea ice salinity. The thermophysical data were collected coincident, in both space and time, with the microwave radiometry data, with the exception of sea ice salinity, which was collected every 48 hours during the winter period.

Ice and snow temperature profiles were measured with 22 AWG, Cu-Co thermocouple junctions. Snow temperatures were measured using 10 equally spaced copper-encased probes at 3-cm intervals from snow-ice interface towards the snow surface. Both sensors and leads were painted white and those leads extending to the logger facility were buried to minimize solar loading. Ice temperature profiles were also measured physically close to the snow profile. A wooden dowel housing 14 thermocouples at varying intervals measured temperature from 1- to 120 cm from the ice surface. This dowel was also painted white for the same reason as the precaution taken for the snow profile and it was frozen into a hole augured in the sea ice. Surface skin temperature was recorded with an Everest 4000 infrared transducer. Further details on this methodology can be found in Mundy *et al.* (2000a).

Snow physical property sampling was performed without replacement in randomly located 0.375-m^2 "snow pits". This procedure was repeated three times a day at approximately 8:00, 13:00 (approximate local solar noon) and 20:00 CST. Pits were dug on the diffusely illuminated snow wall perpendicular to the solar path. Each snow pit measurement consisted of recording snow depth (h_s) and hoar layer thickness to the nearest half cm; hoar layer/snow depth ratios were calculated. Samples used to measure density (ρ_s) were removed at 2-cm intervals with a 66.36-cc density cutter.

Brine volume was calculated for specific points in time according to a pre-existent model by Drinkwater and Crocker (1988). Further details on snow and ice temperature data collection can be found elsewhere (Barber *et al.*, 1994; Mundy, 2000b).

3.4 Data Analysis Methods

3.4.1 Introduction

Based on the objectives introduced in the first chapter and the science rationale discussed on *Chapter 2*, I now present the methods used to analyse the core data of my research. In order to achieve such objectives, statistical tools were used to correlate multiple variables and identify similarities in their seasonal evolution. Qualitative data description was done based on visual assessments of several types of plots, most notably scattergrams and time series plots. Quantitative analysis came from running variances, cluster analysis, and multiple discriminant analysis as well as cross-correlation functions and their coefficients. The results obtained through these analyses are presented on *Chapter 4*.

3.4.2 Seasonal Variance Assessment Through Cluster Analysis

Based on the *Objective 1* requirement of defining seasonal changes on the T_B data, a running variance was calculated on each microwave frequency/polarization signal with the purpose of identifying abrupt changes in variability of the time

series (hereinafter referred to as *break points*). A running term t = 96 was chosen based on the fact that each day had 96 data points (15 min by 24 hours). A new T_B *daily variance* data set was then created.

Using a hierarchical clustering analysis method, the T_B daily variance data were classified with the aim of determining similarities among data points. The choice of a hierarchical cluster analysis was rooted in the fact that this technique has a good performance in dividing previously unclassified data into groups, with significant distance among groups and minimum distance within groups (Everitt, 1980). A *single link method* (or *nearest neighbour*) was used, where the clustering algorithm starts off with groups consisting of single individuals which are successively fused according to the smallest distance between their nearest neighbour. A number of different *a-priori* 'seed' clusters were examined to determine the number of natural clusters existing within the time series. The four-cluster result was significantly better than the exploratory results of 2, 3, 5 and 6 clusters (seeded into the hierarchical analysis). The Mahalanobis distances and associated *p*-value (0.001) show a strong statistical significance for the four-cluster result.

3.4.3 Bivariate Distribution Analysis

Based on the physical temperatures at the surface skin, snow-sea ice interface, and 10cm ice depth layers, emissivities were calculated according to the function presented in [2.11]. This derived variable was used in conjunction with the T_B data in order to assist in evaluating the source and cause of microwave emissions.

Scatterplots were used as a visual assessment tool (Chambers *et al.*, 1983) with the aim of describing the relationship between emissivity (e) and T_B. Since e was derived from T_B, the sole purpose of this visual analysis was to determine the bivariate empirical distribution of both variables, and consequent dependence of these variables on physical temperature.

3.4.4 Multiple Discriminate Analysis

Multiple Discriminate Analysis (MDA) was the approach used to define an optimal channel for characterizing the snow-sea ice system ablation stages, as stated in *Objective 2*. MDA was chosen since it does not require standardized data sets with zero mean and unit variance. As well, it is the proper method to maximize inter-group variation (Manly, 1994). For the purpose of this procedure, the MDA individuals were represented by 6 independent variables (3 frequencies at 2 polarizations) and $N = 4$ groups were selected *a-priori* according to the ablation stages. The MDA calculated N-1 canonical discriminate functions for a maximum differentiation between k *a-priori* groups in a descending order. Hence

the first canonical discriminate axis is orthogonal to the second with minimum residuals and maximum variation between functions. The third follows the same idea, being orthogonal to the second and so do the subsequent functions (Manly, 1986).

Results were corroborated by the *Wilks'* λ statistic, which represents the ratio of the within-groups sum of squares to the total sum of squares. It is a useful test of equality of group means where values close to 0 indicate strong groups differences and 1 indicate no difference among means.

3.5 Summary

In this chapter I presented methods for both data collection and analysis. The data gathering procedures followed techniques used in previous experiments developed during the C-ICE program, hence guaranteeing continuity in the interpretable results. The statistical methods were chosen according to their suitability in comparing different data sets based on the seasonal evolution common to all variables. The output from these analyses led to the results presented and their interpretation in the next chapter.

CHAPTER 4 Results and Discussion

Results pertaining to both objectives presented for this thesis are addressed separately in this chapter. A discussion of the environmental forcing that led to these results follows each section.

4.1 Objective 1

4.1.1 Introduction

My first research objective was subdivided into two interdependent goals: (*a*) to describe the seasonal evolution of microwave emissions at 19-, 37- and 85 GHz V- and H-pol, beginning with a cold snow pack and ending with complete melt pond surface flooding; and (*b*) to explore the statistical relationship between selected thermophysical variables controlling the microwave time series over seasonal periods described in (a).

To address this objective the average temperatures of the air, snow cover-skin surface, snow-sea ice interface and the 10-cm sea ice layer are presented. These temperatures varied considerably over the entire time series, influencing general thermophysical and dielectric properties of the snow-sea ice system. These environmental changes in the snow-sea ice system had a time-lagged effect on T_B

caused by the delay in heat flux as shown on equation [2.6]. The lag effect was assessed by means of cross correlation functions (CCF) for both the winter and ablation 2/3 stages, when enough data were available. Due to lack of sufficient data this analysis was not done for the ablation 1 and 4 stages.

Case studies were done in order to illustrate the most noticeable transitional cases. The cases were characterized on the basis of analysis of the snow-sea ice system water content, brine volume, cloud cover and weather events observed on each day.

4.1.2 Time Series Description

Preliminary assessment of the microwave emission data showed that the T_B time series was of a non-stationary kind with an obvious seasonal component (Figure 4.1.a-b). Little diurnal variability was noticed in T_B early in the season. There was an average of 30K difference in the magnitude of T_B from 19- and 37 GHz to the 85 GHz channel. The 85 GHz channel was more sensitive to weather events (as will be discussed later) but in general its variance was similar to that of the lower frequencies. This result was consistent with previous observations from other investigators, such as Lomax *et al.* (1995), Livingstone *et al.* (1987a), and Grenfell (1986).

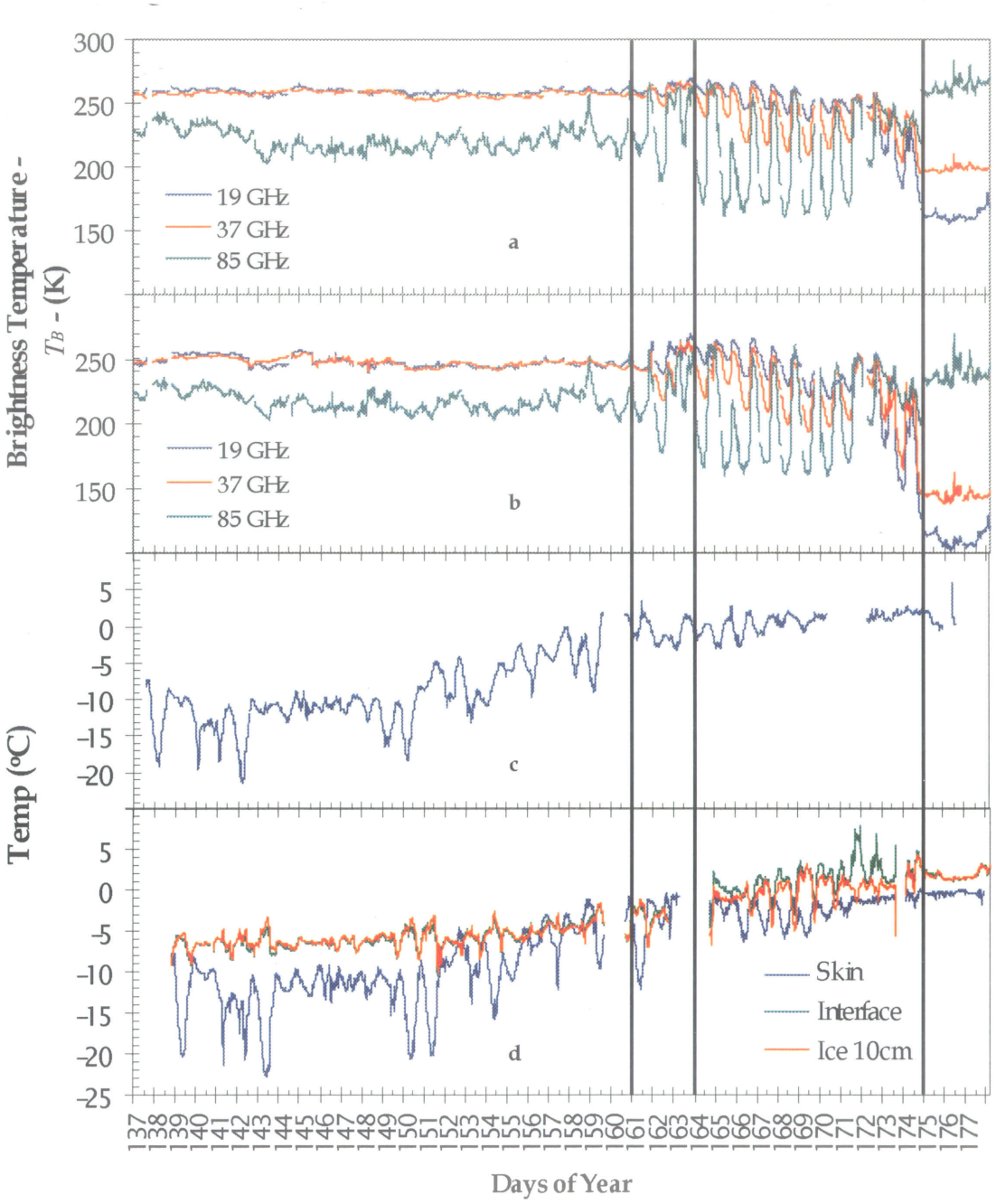

Figure 4.1. Time series plots corresponding to the entire surface-based radiometer (SBR) experiment. (a) Brightness temperature at vertical polarization; (b) brightness temperature at horizontal polarization; (c) air temperature recorded at 2m from surface; (d) temperature profiles at three different locations in the snow/ice volume: skin layer, snow-sea ice interface, and 10 cm from the ice surface. The vertical lines represent the seasonal break points.

There appears to be a strong increase in the diurnal T_B variability starting about day 160. Based on *in situ* observations it is expected that this increase was due to a diurnal cycle in the amount of water in liquid phase present in the snow-sea ice system as a function of air temperature forcing (Figure 4.1.c). The diurnal cycling continues for a substantial period of the time series (day 160 to day 174). The abrupt downward trend in the time series at 19 and 37 GHz occurred at the same period when the surface of the snow-sea ice system was flooded with liquid water. The establishment of the ponding period was quite sudden in 2000 and created a 90% pond- fraction on day 174 in the late afternoon.

These observations led to the conclusion that a strong correlation between T_B and the evolution of the snow-sea ice system seasonal characteristics took place, which in turn were connected to apparent climatic forcing of the snow-sea ice system, hence the need to analyze the data in separate seasons according to its characteristic diurnal variance. An examination of the general conditions of the microwave response and the associated thermophysical variables follows the phenomenological periods description.

Figure 4.2. SBR footprint on day 174 with an estimated 90% melt pond coverage.

4.1.3 Seasonal Variance Assessment

The running variance procedure was performed on all six T_B signals. Each signal had its own running variance curve confirming that, depending on the frequency and polarization, break points would occur in different points along the time series.

In order to allow comparability among frequencies, results from all running variances were averaged into a single running variance signal. Different "seed" clusters were tested with the k-means cluster analysis, which produced best results corresponding to 4 radiometric classes over the full time series. This was expected, and coincident with the ablation stages described by Yackel (2001).

The breakpoints for these clusters corresponded to: *winter*, from day 137 to day 159; *ablation 1*, from day 160 to day 163; *ablation 2/3*, from day 164 to day 174 and *ablation 4*, from day 175 to day 177 (Figure 4.3). This result was interpreted as evidence that the time series microwave data can be used to estimate the timing and duration of each of these 'thermophysical states' of snow covered landfast first-year sea ice.

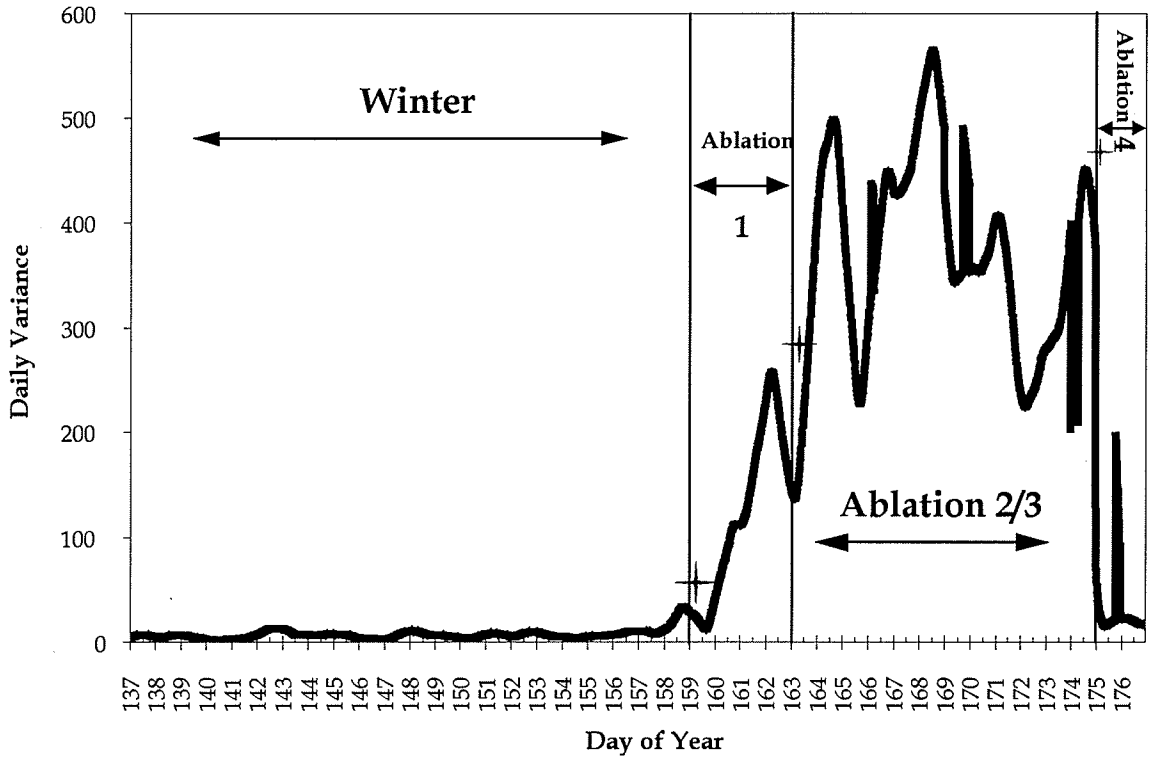

Figure 4.3. Running variance of daily microwave emission variance. Changes in daily microwave emissions are represented by a sudden change in daily variance determining four sea ice ablation periods, from winter to advanced melt. The stars represent points in time defined by a k-means cluster analysis as break points in daily variance. The vertical lines represent the actual breakpoints used in the statistical analysis.

4.1.4 Thermophysical Controls

In this section I discuss the thermophysical controls affecting each of the seasonal stages, from winter to ablation 4.

4.1.4.1 Winter Stage

Ice thickness was approximately 1.5m and was uniformly covered by dry snow varying from 12- to 18 cm in depth. Eppler *et al.* (1992) states that in situations where dry snow cover is present, sea ice is the major source of microwave emissions and the snow cover layer works as an attenuator for emissions coming from the ice, hence being the main factor contributing to the variability of microwave signatures. Results were coincident with this statement and it was found that thicker (> 15cm), less dense snow cover was correlated with lower T_B. A small and constant difference between V pol and H pol (Figure 4.1a-b) was observed.

Microwave time series emission at 19- and 37 GHz had less variance compared with the remainder of the data set. The 85 GHz channel presented larger variance during this stage but was not particularly related to a daily cycle. Observed air temperature was –12°C on average, eventually reaching –5°C by the end of the winter period, with minimal diurnal variation (Figure 4.1c).

Physical characteristics of the snow-sea ice system remained fairly constant while freeze-thaw cycles were not yet taking place. There was a strong temperature gradient in the snow cover caused by the difference in thermal diffusivity of the snow relative to the sea ice.

The cross correlation functions (CCF) shows an immediate response in 85 GHz (V- and H pol) for changes in surface skin temperature, and an approximate 12-hour lag in response to changes in snow-ice interface and ice volume (at 10cm depth). Despite the fact that these results were statistically significant, the correlation coefficients were considered low ($r < 4.5$). As for the 19- and 37 GHz channels, they did not present significant coefficients for CCF between T_B and physical temperature. At this point in time, the weather seemed to be the cause of changes in T_B with more visible variations at 85 GHz, which was found to be the more snow-sensitive channel among the observed frequencies (Comiso *et al.* 1992).

The hoar/snow depth ratio was low – from 0.09 to 0.24 – from day 137 through day 146 (indicative of low snow density). It then increased towards the end of the season reaching values around 0.4. This rise was attributed to increasing volumes of large hoar crystals formed during upward mass transfer due to vapor transport in the snow pack (Barber and Nghiem, 1999).

4.1.4.2 Ablation 1

The period comprising day 160 until 163 was characterized as a transition between winter and ablation 2/3, with a pronounced diurnal cycle in both temperature and phase proportion of water (liquid to solid) in the snow cover. The air temperature was stable near 0°C and the surface skin layer showed freeze-thaw cycles with up to 7°C difference from noon to midnight (Figure 4.1c-d). The snow-sea ice interface and the 10-cm ice layer remained relatively isothermal over the diurnal periods within this 'thermodynamic state' (Figure 4.1.d). The hoar/snow depth ratio changed according to a daily cycle with higher values in the morning and afternoon (around 0.4) and lower in the evening (average 0.25). This corresponded to an approximate 6-hour lag response to increase in atmospheric temperature around solar noon and decreasing temperature during low solar zenith angles (i.e., polar night). The hoar layer was at times not well defined due to the presence of more than one hard ice layer mingled in the snow cover, rendering it difficult to define the exact depth of hoar crystals through visual observation.

Brightness temperature went through an evident diurnal cycle associated with the dielectric properties cycle described in Drobot and Barber (1998) but varied independently from the atmospheric temperature, which remained fairly constant. At this point in time the surface albedo was still high (>85%), but the snow cover could be generally described as damp on the surface with larger grains than in winter. Colbeck (1982) describes an enhancement in snow metamorphism during

the period corresponding to Ablation 1, which leads to an increase in thermal diffusivity of the snow pack. This in turn influences the decreasing length of time it takes for the surface temperature wave to propagate down to the ice surface causing quicker solid to liquid phase changes within the basal snow layer and ice volume, which in turn leads to an increase in brine volume (Figure 4.4).

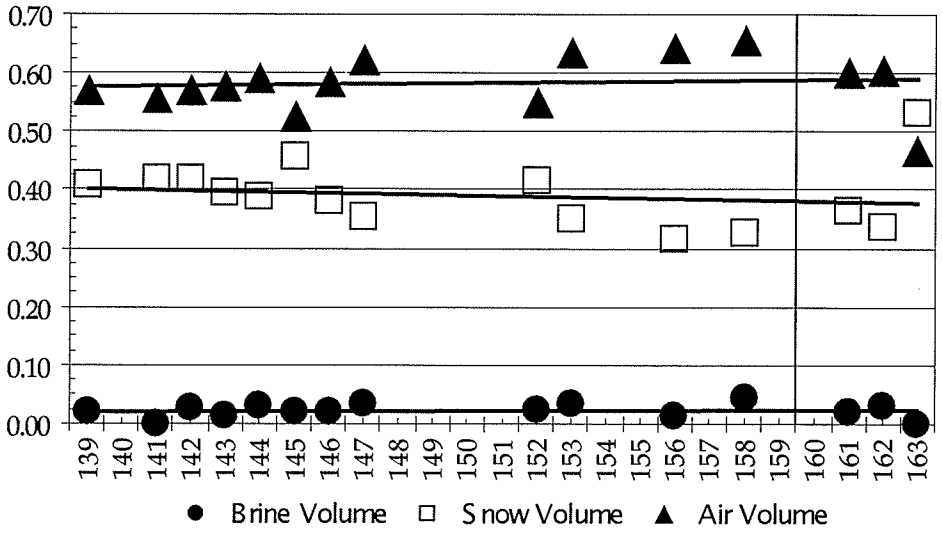

Figure 4.4. Snow brine volume evolution from YD 139 to YD 163. Measurements were made from randomly chosen snow pits.

Water in liquid phase occurred in the system according to a daily cycle. Previous work has shown that the typical values of water in liquid phase during this period ranges from 0% at night to about 5% by volume during the day (Drobot and Barber, 1998). Fung (1994) showed how a small fraction of liquid water (2-4%) mixed with larger metamorphosed snow grains is responsible for a significant increase in emissions. This is coherent with observations, which had higher readings around 6 pm, when wetness was at its peak.

4.1.4.3 Ablation 2/3

Day 164 marked the beginning of the ablation 2/3 cluster, as described by the variability in the microwave response (Figure 4.1.a-b). The ablation 2/3 stage featured a large diurnal variation of absolute values of T_B and stable air temperature with a slight positive trend. By the end of this period the daily air temperature cycle was at a minimum and temperatures remained above zero all day (Figure 4.1.c), contributing to the feedback mechanisms of melt development. A CCF of surface skin temperature and T_B showed that emissions were responding immediately to temperature changes in the skin-surface layer. Higher correlations came from 85V and H pol ($r \approx 0.7$) followed by 37V pol. ($r \approx 0.4$). The snow cover was nearly entirely ablated with only 1- to 2 cm of hard, refrozen ice layer remaining. This metamorphosed layer alone generally contributes to about 20K of the total observed T_B (Lohanick, 1990). The melting process was fed by a decrease in shortwave albedo due to the presence of melt ponds. Small discrete melt ponds were observed in the sampling area at the end of this period but none were immediately within the antenna view of the SBR.

4.1.4.4 Ablation 4

Ablation 4 (starting on day 175) was characterized by lower daily variability with a large range of T_B means (Figure 4.1a-b). Grenfell and Lohanick (1985) pointed out that in this period, microwave emissions from different frequencies yield significantly diverse responses. At this point most of the surface was covered by

interconnected melt ponds up to 10cm in depth, which can be associated with an increase in polarization (Eppler *et al.*, 1992). The skin surface layer temperature showed a small diurnal cycle and stayed above zero for the entire period; the other two temperature sensors at snow-sea ice interface and 10-cm sea ice layers were exposed and thus were not considered reliable at this point. During this period the radiometer field of view consisted of about 80% ponded surface and 20% fully decayed snow. But surface roughness did not appear to play a significant role in the emissions pattern observed, in that on day 175 east winds reached 24 knots causing capillary waves to form on the surface of the ponds but the observed effects of wind forcing on the surface were insignificant. Winebrenner *et al.* (1992) made the same observation with regards to the lack of the emissions' response to minor surface roughness. The remaining two days experienced no wind.

4.1.5 Discussion

Microwave emissions from the snow-sea ice system were found to be dependent on emitted frequency relative to incidence angle, thermophysical characteristics and dielectric properties of the system. Initial analysis on all 6 channels confirmed that each frequency had a particular seasonal variance curve correlated at different strengths with local characteristics of the observed area including, but not limited to the presence of water in liquid phase, physical structure of the ice, and partial fractions of ice, air, and brine occurring in the snow-sea ice system. The higher

diurnal variability was observed during the 11 days corresponding to the ablation 2/3 stage; conversely, the lowest variability occurred during the 24 winter days.

During the winter, emission dependence on thermophysical characteristics of the snow-sea ice system was minimum. The dielectric permittivity and loss did not have significant variance during winter (Drobot, 1997) and T_B was close to constant values for the entire seasonal period. A case study done on day 142 showed a lagged response in T_B relative to climatic forcing of the surface. From mid-day 140 until morning of day 142 atmospheric temperatures fell from –12°C to –21°C when a storm hit the field area. Cloud cover was between $^{8}/_{10}$ to $^{10}/_{10}$ until solar noon, when the storm ended and clear sky was observed for the remaining of the day (Figure 4.5). Brightness temperature at 85V and H pol responded to the new layer of dry snow deposited during the snowstorm with a noticeable decrease in T_B, to which corresponded a consequent decrease in T_B from the snow-sea ice interface and from the ice volume at 10 cm depth. These results agreed with Grenfell (1986), Drobot (1997) and Perovich *et al.* (1998), which confirms the efficiency of dry snow in influencing volume scattering of T_B hence reducing emission. Emissions from 19- and 37 GHz were originated within the sea ice volume and were found to be sensitive to ice surface roughness, but with no apparent correlation with snow cover depth. Both channels presented similar feedback due to the lack of thermophysical and dielectric changes observed in the sea ice volume during the winter. It is known that during this stage the energy

transfer through the high-density sea ice volume is fast, causing small temperature gradients within the volume, which prevents the triggering of sea ice volume thermophysical changes (Papakyriakou, 1999).

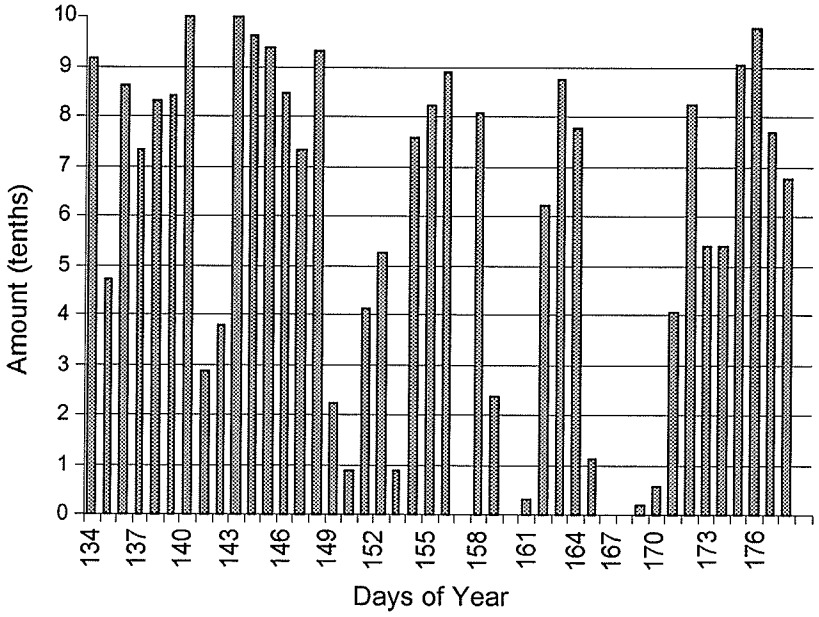

Figure 4.5. Daily average of cloud coverage at the sampling site.

Once the ablation 1 stage started, the daily cycles of water in liquid phase available in the snow-sea ice system occurred mainly in the bottom 4 cm of the snow cover and influenced the dielectric properties of the system, which in turn were found to be highly correlated with T_B fluctuations. Literature has shown that a minimum increase in liquid water content in the snow cover ($\approx$ 1%) triggers a rise in T_B (Gogineni *et al.*, 1992) and results showed that the maximum water volume occurred approximately 13 hours after solar noon. This lagged response to maximum $K\downarrow$ decreased through the 3 days of ablation 1 and on day 163 the maximum T_B reading occurred at 13:30 corresponding to local solar noon. This

result was corroborated by the high CCF coefficients between surface-skin temperature and T_B for V pol frequencies at lag 0 hours ($0.5 \leq r \leq 0.6$). At H pol both 19- and 85 GHz showed high coefficients. The CCF coefficients between physical temperatures at snow-sea ice interface, 10cm-sea ice layer and T_B were also high, but lagged by 13 to 16 hours. This considerable difference in emission response time to changes in $K\downarrow$ and atmospheric temperature was associated with the presence of small amounts of liquid water in the snow-sea ice system causing high stratification and consequent a density gradient in the snow cover volume. According to Barber *et al.* (1995), natural compaction, wind effects, and freeze-thaw cycles contribute to an increase in snow density, mainly in the uppermost layers. Garrity (1992) and Drobot (1997) also observed T_B fluctuations linked to snow cover water content.

The ablation 2/3 stage brought significant daily variance on T_B responses associated with increasing water content (>7%) present in the snow-sea ice system. This can be observed by a downward trend in emissivity means (Figure 4.6) despite the higher oscillation.

A case study was done on day 170. On this day no clouds were observed through the day (Figure 4.5) and air temperature was stable around 0°C. Higher variability for 37- than 19 GHz (Figure 4.7: day 170) was observed. Emissions responded practically immediately to changes in the skin surface temperature at 85GHz

channel ($r \approx 0.7$) and with only 2 hours delay for 37V ($r \approx 0.4$). Figure 4.8 shows the development of a pond on the SBR field of view on days 171 and 172. In 24 hours the pond doubled in area, and depth went from 2-3cm to 8-12cm. In this case, emissions from all channels were all generated on the skin surface, in which case the heat transfer through the sea ice volume is not relevant to T_B readings. The radiometricaly cooler temperatures at 19- and 37 GHz were attributed to the strong control that liquid water has on the emissivity of the surface for the above mentioned frequencies (Jezek *et al.*, 1998) and on the specular nature of the pond surface cover.

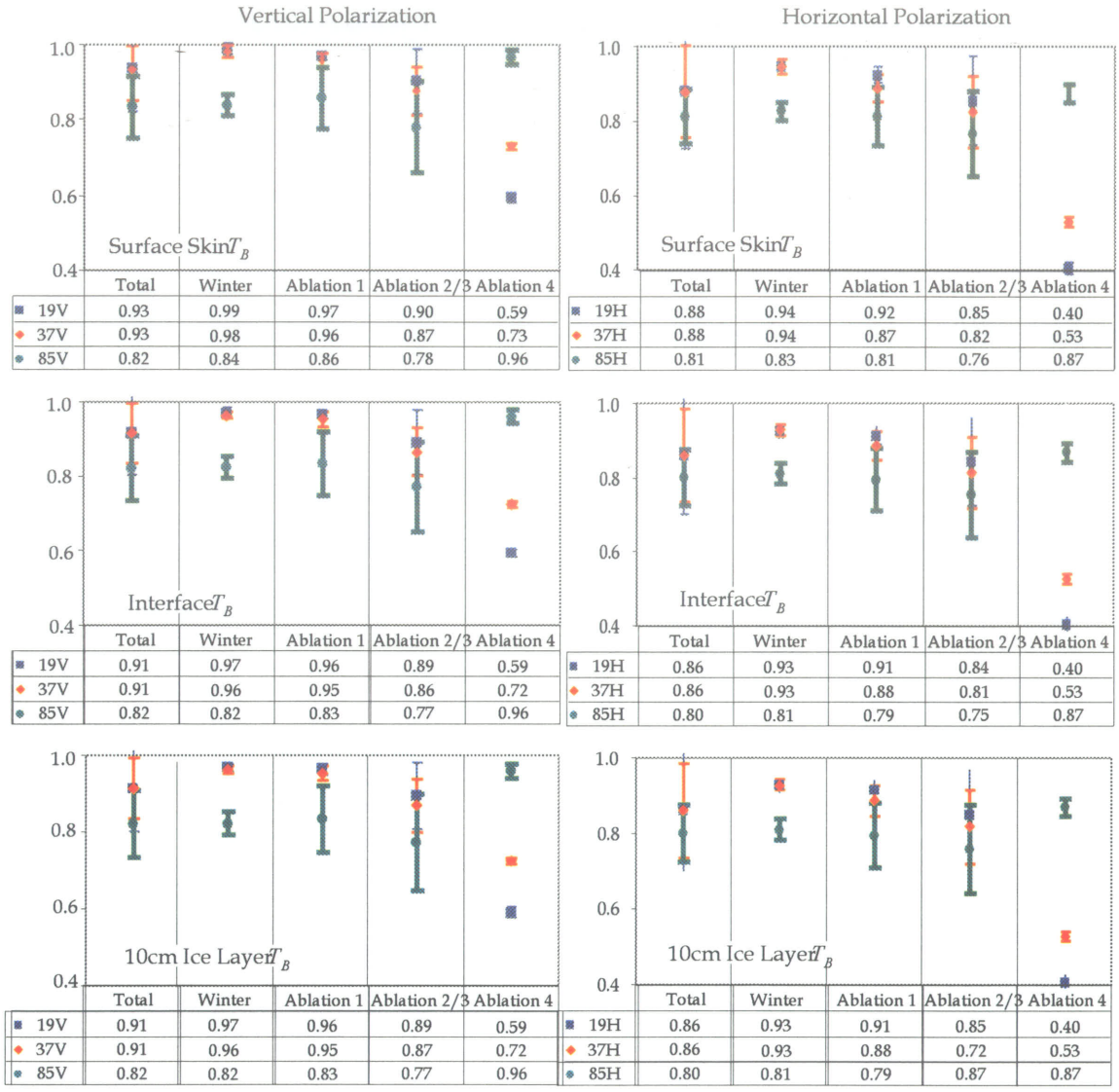

	Total	Winter	Ablation 1	Ablation 2/3	Ablation 4
19V	0.93	0.99	0.97	0.90	0.59
37V	0.93	0.98	0.96	0.87	0.73
85V	0.82	0.84	0.86	0.78	0.96

	Total	Winter	Ablation 1	Ablation 2/3	Ablation 4
19H	0.88	0.94	0.92	0.85	0.40
37H	0.88	0.94	0.87	0.82	0.53
85H	0.81	0.83	0.81	0.76	0.87

	Total	Winter	Ablation 1	Ablation 2/3	Ablation 4
19V	0.91	0.97	0.96	0.89	0.59
37V	0.91	0.96	0.95	0.86	0.72
85V	0.82	0.82	0.83	0.77	0.96

	Total	Winter	Ablation 1	Ablation 2/3	Ablation 4
19H	0.86	0.93	0.91	0.84	0.40
37H	0.86	0.93	0.88	0.81	0.53
85H	0.80	0.81	0.79	0.75	0.87

	Total	Winter	Ablation 1	Ablation 2/3	Ablation 4
19V	0.91	0.97	0.96	0.89	0.59
37V	0.91	0.96	0.95	0.87	0.72
85V	0.82	0.82	0.83	0.77	0.96

	Total	Winter	Ablation 1	Ablation 2/3	Ablation 4
19H	0.86	0.93	0.91	0.85	0.40
37H	0.86	0.93	0.88	0.72	0.53
85H	0.80	0.81	0.79	0.87	0.87

Figure 4.6. Emissivity means from three different sources for all observed seasons at 19-, 37-, and 85GHz V- and H pol.

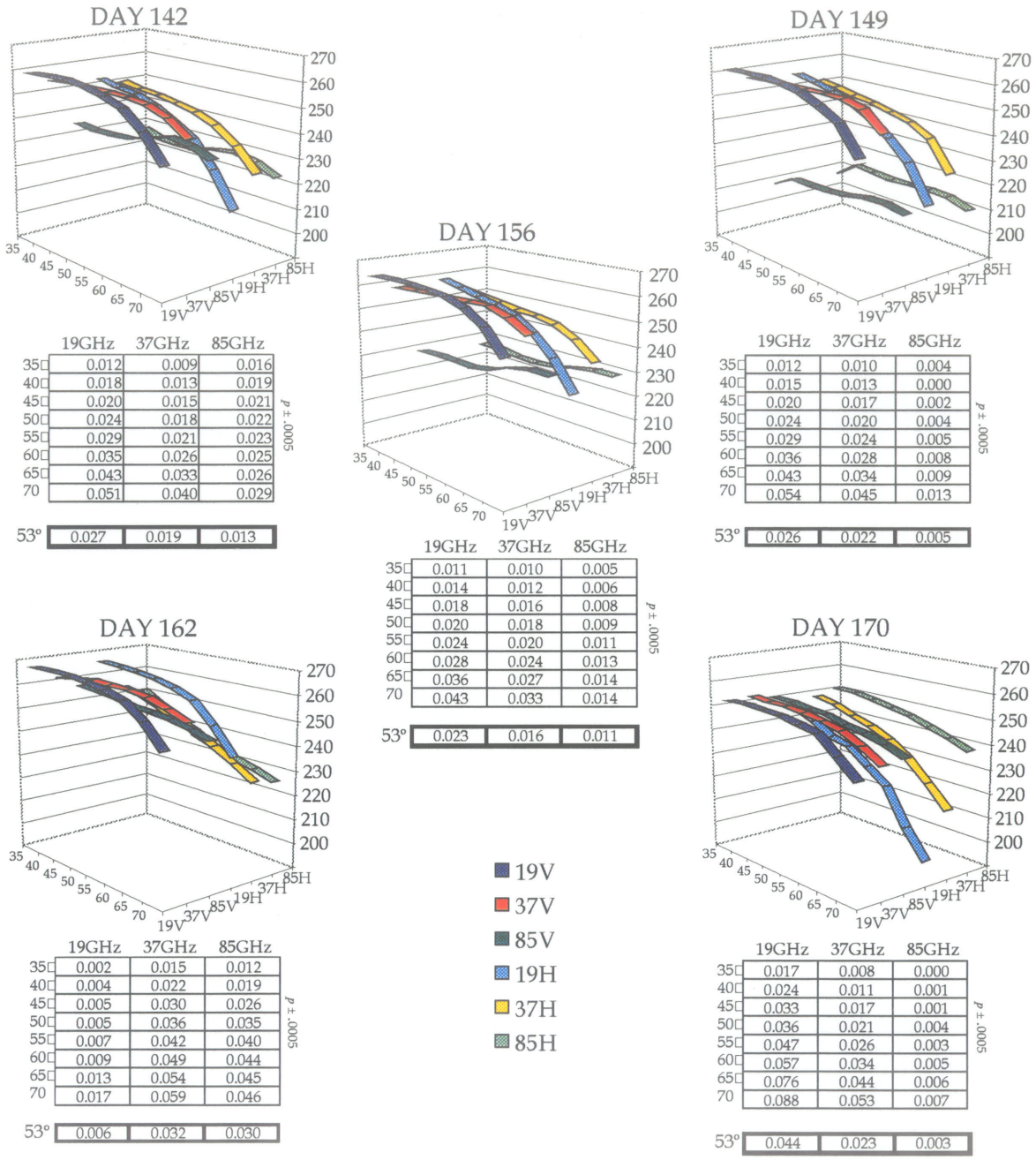

Figure 4.7. Distinct case studies for T_B versus incidence angle and frequency. The graphs above snow T_B's angular dependence and the evolution of polarization relative to seasonal changes.

Based on the incidence angle replicate sampling data set it was possible to analyze the T_B's angular dependence; as well as changes in polarization at each frequency defined as $p = [(T_{B_V} - T_{B_H})/(T_{B_V} + T_{B_H})]$. Figure 4.7 shows the evolution of polarization versus incidence angle throughout the experiment and it was found that variations increase at lower frequencies. This was attributed to the fact that most of the lower-frequency emissions come from deeper in the sea ice volume during winter and ablation 1, where subsurface ice structure influences polarization. For ablation 2/3 and 4, 19GHz is still more polarized than 85 GHz but at this time the larger variance was attributed to the lower-frequency sensitivity to pond surface changes due to freeze-thaw cycles combined with emissions from the underlying melt pond water. That is, in cases where an optically thin ice layer was formed on the melt pond surface, the high reflectivity of the underlying melt pond water influenced the emissions on lower frequencies but did not affect 85 GHz, which was only sensitive to the overlying ice layer. Hence emissions on 19- and 37GHz represented an integration of both media: ice and liquid water. For all case studies analyzed, higher incidence angles yielded more polarized results.

From a temporal perspective, polarization tended to decrease with the seasonal evolution. An interesting anomaly was observed on day 162 for both 37- and 85 GHz, where p values went up in an otherwise decreasing trend. This was a characteristic ablation 1 day, when ice layers were found in the snow cover

volume at 2- and 6cm from the sea ice surface causing high polarization even at the highest frequency observed. These interpretations led to the science question presented in Objective 2: which one of the 3 observed frequencies at V- and H pol would yield better results in accounting for the largest amount of variance in the seasonal evolution of the snow-sea ice system. The results pertaining to this objective will be discussed on the following section.

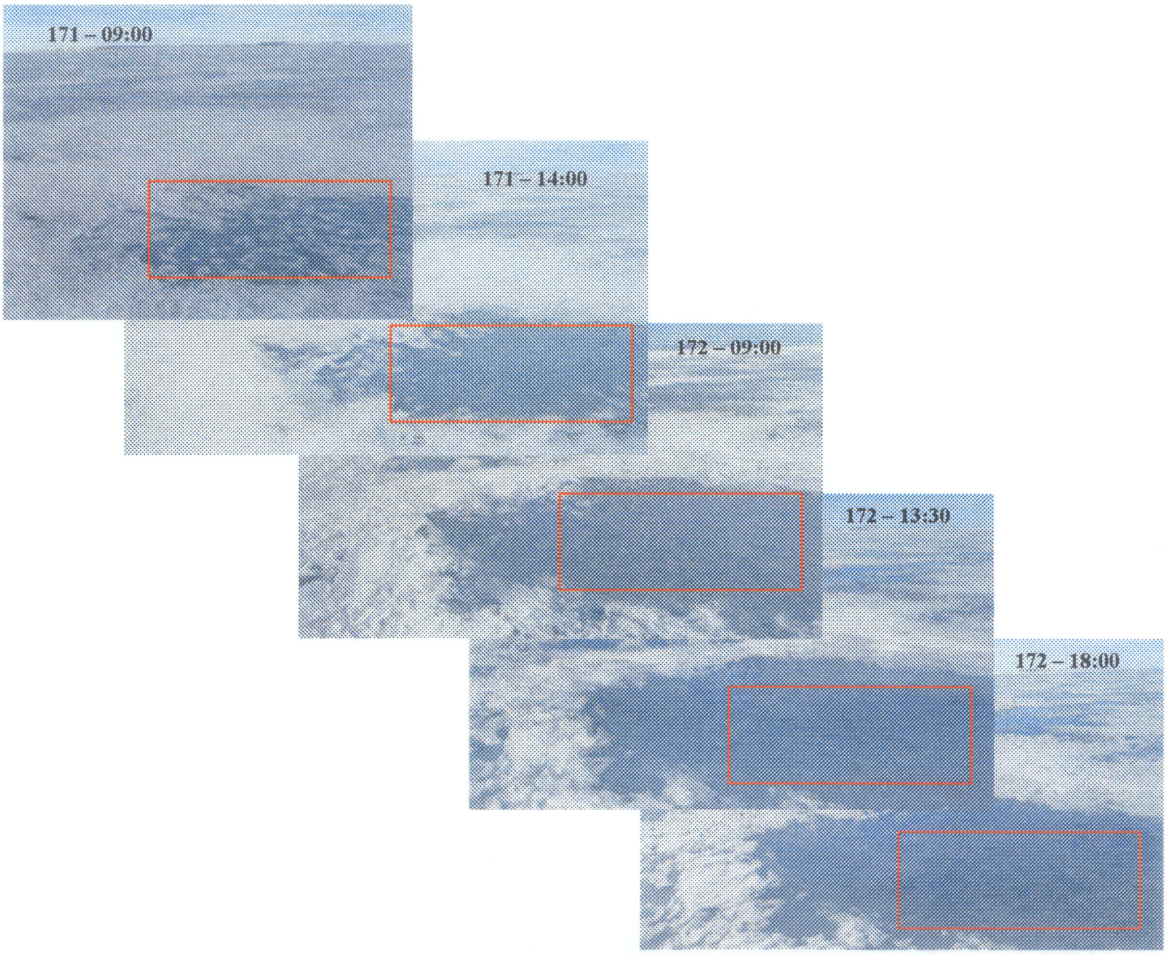

Figure 4.8. Pond evolution in a 24-hour period on days 171 and 172. The red rectangle illustrates the increasing area of the pond relative to the first scene. These photos represent the SBR field of view.

4.2 Objective 2

4.2.1 Introduction

The second thesis objective is now restated: to assess the utility of the three analyzed microwave frequencies at both polarizations and to define which of the channels or combination of channels provide a better characterization of the sea ice ablation stages. This objective was approached by means of a Multiple Discriminate Analysis (MDA). This classification procedure was aimed at defining an outstanding frequency in terms of explaining the largest amount of thermophysical variance in microwave emissions from the sea ice volume over the time series.

The idea of classifying the T_B data was based on the fact that different frequencies respond differently to changes in the dielectric properties of sea ice relative to its ablation states (as described above).

4.2.2 Classification of the Variance

The goal for the brightness temperature classification was to rank the six channels according to how much of the total T_B seasonal variance is accounted for at each frequency. Table 4.1 shows that both 19V and 37H had very high correlation coefficients with the *discriminant function 1* (DF1), which in turn responded for 70.8% of the total variance.

The cumulative variation of both DF1 and DF2 (orthogonal axes) accounted for 92.9% of the total variation (Table 4.2). Hence both 19V and 37H were considered as the best discriminator variables.

Table 4.1. Pooled, within-group, correlations between discriminating variables and standardized canonical discriminant functions obtained from the MDA results.

	DISCRIMINANT FUNCTIONS		
	1	2	3
19V	**.902***	-.142	.329
37H	**.900***	.011	.013
19H	**.886***	-.222	.364
37V	**.806***	.270	.062
85V	-.214	**.381***	-.030
85H	-.100	**.294***	-.120

* Largest absolute correlation between each variable and any discriminant function.

It followed that 19H and 37V also presented high correlations with DF1, whereas both 85 GHz channels had some small correlation with DF2 but no significant correlation with DF1. This was interpreted as excessive sensitivity at 85GHz for the overall seasonal transition.

Table 4.2. Eigenvalues and percentage of variance for the first 3 canonical discriminant functions used in the analysis.

Discriminant Function	Eigenvalue	% of Variance	Cumulative %	Canonical Correlation
1	4.705	70.8	70.8	.908
2	1.471	22.1	93.0	.772
3	.466	7.0	100.0	.564

Figure 4.6 shows that throughout the snow-sea ice system ablation period the 85 GHz V and H emissivity means do not vary as much as the other two channels, rendering it less useful in determining changes in snow-sea ice properties.

Again, the 19- and 37V and H signals showed significantly low *Wilks' λ* values (ratio of the within-group sum of squares to the total sum of squares), confirming the high variability among groups. The F statistic (ratio of between-groups variability to the within-groups variability) showed that the variability among groups is significantly higher than within groups for 19- and 37 GHz.

Table 4.3. Test of equality of group means.

	Wilks' λ	F	degrees of freedom 1 (N-1)	degrees of freedom 2 (valid cases)	Significance ($p \leq 0.001$)
19V	.204	4855.523	3	3729	.000
19H	.207	4755.377	3	3729	.000
37V	.240	4740.424	3	3729	.000
37H	.208	3930.978	3	3729	.000
85V	.700	533.262	3	3729	.000
85H	.847	224.711	3	3729	.000

4.2.3 Discussion

Large fluctuations in microwave emissions were observed throughout the experiment. Such variability was found to be correlated with changing dielectric properties of the targeted area, which comprises both the snow and sea ice volumes. Figure 4.9 shows that emissivities originating in the skin surface, snow/ice interface, and at 10 cm depth into the ice volume are positively

correlated with the T_B for the entire time series period but with different data clustering relative to the ablation season. Observed clusters in the data distribution indicate that T_B doesn't always respond directly to changes in emissivity. This was expected, especially within the winter period. This can be shown by the fact that, during the winter, dry snow works as a scatterer for emissions coming from the lower layers, but it still enables some energy to permeate. Hence, variability in the snow cover affects emissivity, but does not affect T_B. For both the 19- and 37GHz channels T_B values above 220K were characteristic of the winter stage. By observing the data clustering pattern in Figure 4.9, it is possible to infer that there is a low correlation between emissivity e and T_B which implies that emissivity variations were not dominant in the relationship described at equation [3.3] during the winter. Once water in liquid phase was present, all emissions originated at or near the surface and at this point, changes in the data clustering were then attributed to sensitivity of the surface emissivity to the formation of moisture between snow grains. It was observed that small amounts of moisture (up to 5%) resulted in increasing emissions, but once moisture is present in larger volumes, T_B tends to go down due to the radiometricaly cold characteristic of melt ponds. Results from the entire data distribution showed that, when comparing 19- and 37GHz measurements, the data clustering at 37GHz showed distinct clusters associated with T_B intervals, which in turn are characteristic of ablation stages.

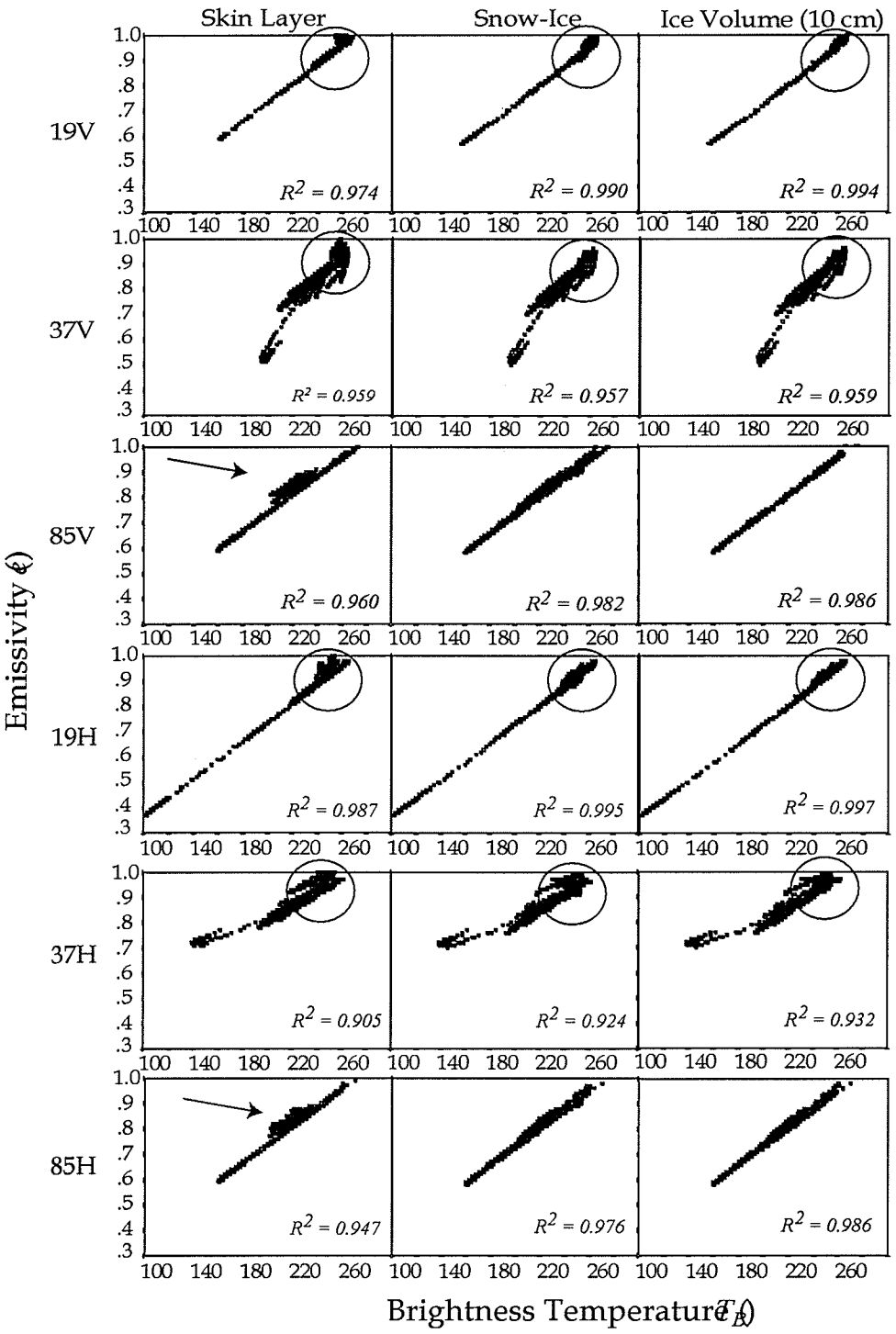

Figure 4.9. Scatter plots of emissivities versus T_B at three different layers: skin layer; snow-ice interface, and ice volume at 10cm (R^2 was calculated based on a 99% confidence level).

For the 85 GHz channel (V and H) a combined analysis of the results from Figure **4.1**a-b and Figure 4.9 show that the majority of the data points corresponded to T_B values between 190K and 220K independent from ablation stage.

It was than observed that emissivities from the surface skin layer are less correlated with T_B at the same interval than at the remaining data points. Based on these observations it was possible to conclude that, during this experiment, the contrast between dry ice and water was lower at 85GHz, hence the magnitude of the decrease in T_B due to melt pond formation was greater at lower than higher frequencies. This observation corroborates results presented by Comiso and Kwok (1996).

Objective 2 was achieved by determining that, based on this data set, 37GHz at V- and H pol accounted for more T_B variance than the 19- and 85GHz channels. Between the latter two channels, 85 GHz was the one with the poorest performance in accounting for variance, and therefore least suitable for helping to differentiate among ablation stages.

4.3 Summary

The results presented in this chapter were aimed at achieving both objectives stated in Chapter 1. The T_B data set collected during the C-ICE 2000 experiment was successfully described based on the seasonal evolution of thermophysical and dielectrical characteristics of the snow-sea ice system. I discussed the changes observed in the sea ice snow cover due to weather events and melt processes and how such changes directly or indirectly affected the snow-sea ice system microwave emissions. Based on the data available for this research, I identified incoming shortwave radiation ($K\downarrow$) as the triggering factor in the seasonal evolution process and the lagged effect of energy transfer through the snow-sea ice system, and the corresponding microwave emissions.

Objective 2 was achieved by means of a Multiple Discriminant Analysis with the aim of identifying which of the six observed channels accounted for the most variance in the data set. This, therefore, suited the purpose of remotely assessing the snow-sea ice system seasonal evolution based on microwave radiometry.

CHAPTER 5 Summary and Conclusions

5.1 Thesis Summary

In the first chapter I introduced the concept of snow and sea ice as two parts of an integrated system, which by means of feedback mechanisms interacts with the overlying atmosphere and the underlying ocean in the ocean-sea ice-atmosphere interface. I described this system as the main constituent of the marine cryosphere, which in turn is an integral component of the global climate system. I then linked Arctic climate variability and change with the overall energy balance in polar regions as a function of sea ice extent. I introduced passive microwave radiometry as a viable tool for the assessment of the snow-sea ice system. The two thesis objectives were stated in the context of polar climate research as a proxy to understanding arctic climate change.

In *Chapter 2* I presented the scientific background for this research by describing the thermophysical and dielectric properties of the snow-sea ice system according to the seasonal evolution observed in the Arctic. I portrayed the changes in the energy balance of the ocean-sea ice-atmosphere interface as the triggering factor for the onset of the snow-sea ice system ablation, which results in changes in the thermophysical and dielectric characteristics of the system. I then described the

connection between passive microwave emissions with seasonal transitions. This chapter ended with a description of the passive microwave interactions in the snow-sea ice system and a discussion of the application of microwave radiometry for the analysis of the marine cryosphere.

In *Chapter 3* I described the procedures and equipment used for field data collection, with special attention given to the operation and calibration of the surface-based radiometer (SBR). I also introduced the statistical tools used for the data analysis, with a brief description on why each tool was chosen.

In *Chapter 4* I incorporated the theory presented in the second chapter with the methods used for data collection and analysis, producing results linked to both research objectives presented in *Chapter 1*. I presented an extensive description of the evolution of microwave emissions from a fixed point in the snow-sea ice system, correlating the changes observed in daily variance to *in situ* environmental observations, such as snow-melt pond fraction, presence of water in liquid phase and air temperature oscillations. Different microwave channels yielded different results, which led to the argument that, based on the data collected, an optimal channel for snow-sea ice system observation could be determined. With the use of multi-discriminant analysis, all channels were classified according to the amount of variance in each set of microwave emissions.

5.2 Conclusions

In the introduction chapter the following general science objective was presented:

Science Objective: "To describe the seasonal evolution of smooth, fast, first-year sea ice using microwave radiometry and to assess the applicability of different microwave frequencies in characterizing sea ice seasonal ablation states."

This statement was subdivided into two interdependent objectives as follows:

Objective 1. (*a*) To quantitatively and qualitatively describe the seasonal evolution of microwave emissions at 19-, 37- and 85 GHz V and H polarizations, beginning with a cold snow pack and ending with complete melt pond surface flooding; and (*b*) to explore the statistical relationship between selected thermodynamic and geophysical variables controlling the microwave time series over seasonal periods described in (a).

Objective 2. To assess the utility of the three analyzed microwave frequencies (19-, 37-, and 85 GHz) at both polarizations (V- and H pol) and to define which of the six channels or combination of channels provide an optimal characterization of the snow-sea ice system ablation states.

Based on the results presented in *Chapter 3*, the following conclusions can be drawn:

① Microwave emissions from the snow-sea ice system are sensitive to changes in the thermophysical and dielectric characteristics of the volume as a function of seasonal evolution. This becomes evident by analyzing the T_B signal and observing its non-stationary characteristic with an obvious seasonal component. One of the triggering variables for the seasonal change phenomena is the input of shortwave radiation ($K\downarrow$) to the system, which in turn affects the energy balance in the ocean-sea ice-atmosphere (OSA) interface, and then influencing the thermophysical and dielectric properties of the snow-sea ice system. More research is necessary in order to properly identify other triggering mechanisms for the seasonal evolution.

② Each microwave frequency responds differently to seasonal transitions. The amount of variance observed in each frequency is a function of the depth from which the emission is being generated, the snow-sea ice system surface physical characteristics, and emission polarization. These three components are inter-dependent.

The shorter wavelength corresponds to the 85 GHz channel and emissions at this frequency are originated in the surface-skin layer. Therefore an increase in water in liquid phase at the surface-skin as low as 1% is sufficient to cause

variance in the emissions. As for both the 19- and 37 GHz channels, the larger variance in emissions is observed as a function of the physical structure of the volume, which in turn augments the polarization of the emission. Since most of the emissions come from 10- to 15 cm below the surface, once melt ponds are formed, the specular characteristic of the pond surface prevents the bulk of the emitted energy to reach the antenna.

③ Temperature changes and consequent freeze-thaw cycles in the snow-sea ice system have a time-lagged effect on T_B as a function of the delay in heat flux through the system. During the winter, due to the lack of water in liquid phase, changes in temperature do not correlate with changes in emissions; in fact, the amount and density of deposited snow on the sea ice is what determines the observed emissions. Once there is a diurnal cycle in the amount of water in liquid phase present in the system, a strong increase in diurnal variability of T_B is observed. At this point there is a delayed T_B response, which is a function of the diurnal cycle in thermophysical and dielectric properties within the snow-sea ice system.

④ Passive microwave radiometry data can be used to estimate the timing and duration of each thermophysical state of the snow-covered landfast first-year sea ice. The optimal frequency to determine variations in the thermophysical properties of the snow-sea ice system is that which accounts for the most variance in the T_B signal throughout the entire seasonal evolution period, with

evident correlations to *in situ* seasonal transitions. The 37 GHz frequency, at both polarizations, was found to be the most consistent in representing transition stages in the snow-sea ice system without being excessively sensitive to the variability of surface characteristics. Conversely, the 85GHz channel was found to be excessively insensitive to subtle thermophysical changes in the observed area. The 19 GHz channel showed similarity to the 37 GHz channel, in terms of how efficiently it accounted for seasonal changes. Nevertheless, at times, the response given by the 19 GHz channel to subtle alterations in the environment, such as the overnight formation of a thin ice layer on the surface of melt ponds, was not detectable.

5.2.1 Links to Remote Sensing

Given the fact that the marine cryosphere is a good early indicator of global climate variability and change, quantifying the amount and characteristics of change observed in both the North and South poles is important in determining the extent of such environmental changes. Based on this context, results pertaining to *objective 1* showed that microwave radiometry data collected from a surface-based sensor were indeed sensitive to the snow-sea ice system seasonal evolution and therefore useful in defining sea ice ablation states. Changes in the thermophysical and dielectric properties of the snow-sea ice system were strongly correlated with the microwave radiometry data. In order to understand how the snow-sea ice system conditions influence T_B, I discussed the need to gather good quality data on

ice extent and thickness, snow depth, summer melt, melt pond coverage, and weather and ocean forcing on these variables.

Following the assumption that a surface-based microwave radiometer can collect high spatial and temporal resolution data from a fixed area, one of its applications would be spaceborne data validation of already-operational sensors. The thermophysical and dielectric information derived from such experiments can be later used in developing algorithms for future sensors. In addition to that, the SBR experiment can be useful in understanding how spaceborne data at regional and inter-annual time scales can be used in climate research.

The choice of frequencies used in this SBR experiment was based on the Special Sensor Microwave/Imager (SSM/I) operational since 1992. The SSM/I sensor operates on board each of the Defense Meteorological Satellite Program (DMSP) satellites. These platforms operate in a near-polar, sun synchronous orbit with an orbital period of 101 minutes at a nominal altitude of approximately 830 km above the Earth; it crosses any point on the Earth up to two times a day. Of all channels available in this system, the smaller footprint comes from the 85 GHz channel with 13 x 15 km and the largest corresponds to the 19 GHz channel with 43 x 69 km. One of its main purposes has been the retrieval of sea ice T_B at 19.35-, 37.0-, and 85.5 GHz, and at both vertical and horizontal polarizations (DMSP, 2001). Scheduled for launch in early 2002 is a second microwave imager (Advanced Microwave Scanning Radiometer - AMSR) operating at frequencies 18.7-, 36.5-,

and 89.0 GHz, with the largest footprint corresponding to the 18.7GHz channel (43 x 5 km) and the smallest corresponding to the 89.0Ghz with 3.5 x 5.9 km. This sensor will be installed in a platform operating at a nominal altitude of 705 km with orbital period of 98.8 minutes and covering the entire globe every 16 days (AMSR, 2001).

5.3 Limitations and Future Directions

Due to the extreme environmental conditions where this research was performed, some limitations were imposed on the project and at some points data quality improvement is recommended. In what follows I describe observed limitations and suggest alternatives to problems previously encountered. Next I introduce possible future directions with some particulars as to the direction in which this research should evolve.

The fundamental principal of using remote sensing techniques to deduce present characteristics of a given environment is based on the correlation existing between the remotely sensed data and the surface validation data collected through *in situ* field experiments. Hence, the quality of the ancillary data set containing geophysical and dielectric variables observed in the environment is of the utmost importance. Therefore, future work must consider it a priority to collect thorough ancillary data sets of snow and sea ice physical temperatures at the surface and within the snow and ice volumes. The most conspicuous characteristics that

influence the microwave emissions, and thus require special attention, are: snow density, water in liquid phase, area and depth of melt ponds, and presence of refrozen ice layer in the snow volume or on the surface-skin layer. Hence, it is highly recommended that the actual physical conditions encountered in the observed area should be recorded in order to systematically facilitate more detailed analysis. In order to properly associate seasonal transition periods in the snow-sea ice system with the observed microwave signal, a methodical description of the antenna field of view is worthy of note.

With regards to the SBR operational quotidian, several potential sources of calibration error were identified: radiometer pointing error, uncertainties in terms of water vapor present in the air, random system noise, and uncertainties relative to the measurement of the blackbody temperature. For future research these errors should be brought to a minimum rendering the data set useful not only for relative calibrated assessments of the snow-sea ice system, but also for accurate descriptions of the sensor performance itself.

In order to further refine the surface validation of the snow-sea ice system ablation stages it is important to keep the SBR system operational for as long as possible, covering all possible transition stages observed on snow-covered first-year sea ice. However, once the melt season progresses, the mere deployment of the SBR becomes a source of error. That is because keeping the system afloat on constantly increasing melt ponds may cause artificial disturbance on the field of

view and lack of stability in the system itself, which will eventually spoil the precision of the calculation of the field of view. In order to minimize this problem it might be worth considering having the SBR system deployed over two separate sledges. The first sledge would support the controlling system stored in weatherproof housing, the heavier part of the SBR system. This therefore, can stay still and in one position regardless of potential melting and refreezing underneath the it. The second sledge would support the SBR antenna boxes and tripod. This sledge should be lighter in weight and consequently easier to move (Figure 5.1).

Thus, it would be possible for the operational team to move the SBR every 12 hours, if necessary, to make sure the system is leveled and stable.

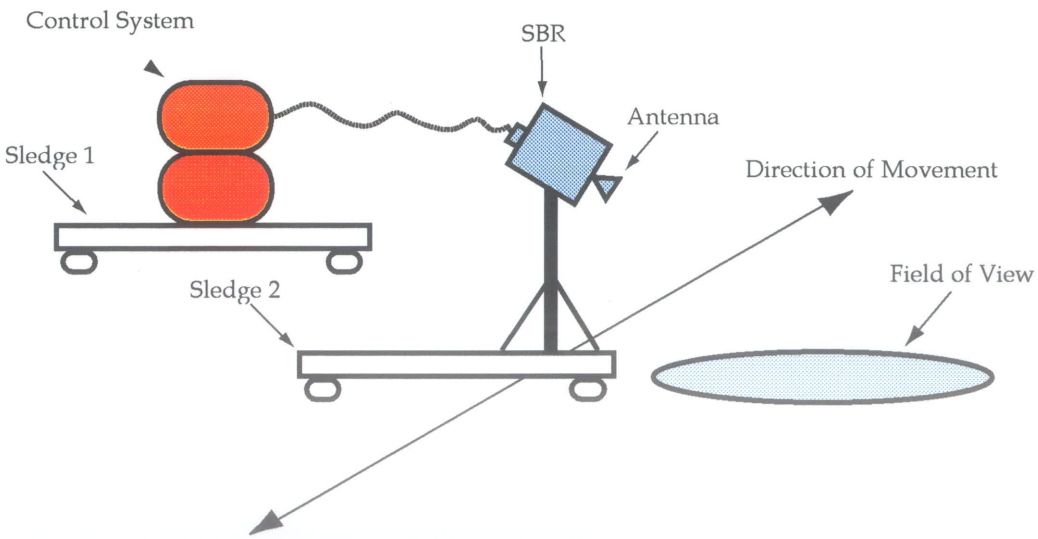

Figure 5.1. Schematic description of a potential deployment for the SBR system.

This set-up should be enough to minimize the radiometer pointing error and, together with a systematical recording of the local physical conditions, the data analysis should be facilitated.

Based on the data analysis covered in this thesis, it is possible to say that promising areas exist for further research in passive microwave signal analysis. Research can be done on improving the correlations between the actual satellite data, potentially AMSR data, and the SBR data. For that purpose it is important to understand the effect caused by the atmosphere as a potential source of scattering and absorption of emitted microwave energy. Additionally, research in transition areas, such as the ice edge and polynyas, should be carried out in order to improve the current knowledge on the different microwave emissions from the ice-water interface.

Finally, due to the time-dependence of this data set, this work could be further developed by using alternative mathematical tools, such as Fourier and wavelet analysis, in order to gain a better perspective on alternative characteristics of the data.

Cited References

Advanced Microwave Scanning Radiometer – AMSR. 2001. Sensor Characteristics. [report on-line] National Space Agency of Japan, accessed 18 December 2001; available from http://sharaku.eorc.nasda.go.jp/AMSR; Internet.

Asmus, K. and I. Harouche. 2000. "Section 3.2. Surface-Based Radiometer Experiment," in C-ICE 2000 Field Summary. CEOSTEC-2000-12-01, *ed.* Iacozza, J. and D.G. Barber. Winnipeg, MB, pp. 102-113.

Barber, D. G., D. G. Flett, R. A. DeAbreu, and E. F. LeDrew. 1992. "Spatial and temporal variations in sea ice geophysical properties and microwave remote sensing observations: the SIMMS'90 experiment," *Arctic*, vol. 45, no.3:233-251

_____, T.N. Papakyriakou, and E.F. LeDrew. 1994. "On the relationship between energy fluxes, dielectric properties, and microwave scattering over snow covered first-year sea ice during the spring transition period," *Journal of Geophysical Research*, vol. 99, no. C11: 22,401-22,411.

_____, S. P. Reddan, and E. F. LeDrew. 1995. "Statistical characterization of the geophysical and electrical properties of snow on landfast first-year sea ice," *Journal of Geophysical Research*, vol. 100, no. C2: 2673-2686.

_____, A.K. Fung, T.C. Grenfell, S.V. Nghiem, R.G. Onstott, V.I. Lytle, D.K. Perovich, and A.J. Gow. 1998. "The role of snow on microwave emission and scattering over first-year sea ice," *IEEE Transactions on Geosciences and Remote Sensing*, vol. 36, no. 5: 1750-1763.

_____ and S. V. Nghiem. 1999. "The role of snow on the thermal dependence of microwave backscatter over sea ice," *Journal of Geophysical Research*, vol. 104, no. C11: 25,789-25,803.

_____ and J. J. Yackel. 1999. "The physical, radiative and microwave scattering characteristics of melt pond on sea ice," *International Journal of Remote Sensing*, vol. 20: 2069-2090

_____, J. J. Yackel, and J. M. Hanesiak. 1999. Sea Ice Decay for Marine Navigation – Final Report. CEOSTEC-10-1-99. Winnipeg, MB, 148pp.

Barry, R. G. 1983. "Arctic ocean ice and climate: perspectives on a century of polar research," *Annals of the Association of American Geographers*, vol. 73, no. 4:485-501.

_____., M. C. Serreze, J. A. Maslanik. 1993. "The Arctic sea ice-climate system: observations and modeling." *Reviews of Geophysics*, vol. 31, no. 4: 397-422.

_____. 1996. "The parameterization of surface albedo for sea ice and its snow cover," *Progress in Physical Geography*, vol. 20: 63-79.

Brown, R. D. and P. Cote. 1992. "Interannual variability of landfast ice thickness in the Canadian High Arctic, 1950-89," *Arctic,* vol. 45, no. 3: 273-284

Budyko, M. I. 1969. "The effect of solar radiation variations on the climate of the Earth," Tellus, vol. 21: 611-624.

Canadian Ice Service (CIS). 2001. "Ice terminology," [document on-line], accessed 15 September 2001; available from http://ice-glaces.ec.gc.ca/; Internet.

Carsey, F. D. 1985. "Summer Arctic sea ice character from satellite microwave data," *Journal of Geophysical Research,* vol. 90, no. C3: 5015-5034.

_____., R. G. Barry, and W. F. Weeks. 1992. Introduction to Microwave Remote Sensing of Sea Ice. Geophysical Monograph 68, *ed.* F. Carsey. Washington, DC: American Geophysical Union, pp. 1-6.

Chambers, J.M., W.S. Cleveland, B. Kleiner, P.A. Tukey. 1983. Graphical Methods for Data Analysis, Boston, MA: Duxbury Press, 395pp.

Colbeck, S.C. 1982. "An overview of seasonal snow metamorphism," *Reviews of Geophysics and Space Physics,* vol. 20: 45-61.

Comiso, J. C. 1983. "Sea ice effective microwave emissivities from satellite passive microwave and infrared observations," *Journal of Geophysical Research*, vol. 88, no. C12: 7686-7704.

_____. 1985. "Remote sensing of sea ice using multispectral microwave satellite data," in Advances in Remote Sensing Retrieval Methods., *eds.* A. Deepak, H. E. Fleming, and M. T. Chahine. Hampton, Virginia: Deepak Publishing, pp. 349-359.

_____., T. C. Grenfell, M. Lange, A. W. Lohanick, R. K. Moore, and P. Wadhams. 1992. "Microwave remote sensing of the southern ocean ice cover," in Microwave Remote Sensing of Sea Ice. Geophysical Monograph 68, *ed.* F. Carsey. Washington, DC: American Geophysical Union, pp. 243-259.

_____. and R. Kwok. 1996. "Surface and radiative characteristics of the summer Arctic sea ice cover from multisensor satellite observations," *Journal of Geophysical Research*, vol. 101, no. C12: 28,397-28,416.

Cox, G. F. and W. F. Weeks. 1975. Brine Drainage and Initial Salt Entrapment in Sodium Chloride Ice, CRREL Research Report 385, Hanover, NH: Cold Regions Research and Engineering Laboratory, 85pp.

Crocker, G. B. 1984. "A physical model for predicting the thermal conductivity of brine wetted snow," *Cold Regions Science and Technology*, vol. 10: 69-74.

Defense Meteorological Satellite Program - DMSP. 2001. Description of DMSP Sensors. [report on-line] National Oceanic and Atmospheric Administration, accessed 18 December 2001; available from http://www.ngdc.noaa.gov/dmsp/; Internet.

Drinkwater, M. R., and G. B. Crocker. 1988. "Modelling changes in the dielectric and scattering properties of young snow-covered sea ice at GHz frequencies, *Journal of Glaciology*, vol. 34, no. 118: 274-282.

Drobot, S. D. 1997. Microwave radiometry and snow water equivalence retrievals on snow covered sea ice in the marine cryosphere. (Master of Arts dissertation, University of Manitoba)

_____ and D. G. Barber. 1998. "Towards development of a snow water equivalence (SWE) algorithm using microwave radiometry over snow covered first-year sea ice," *Photogrammetric Engineering and Remote Sensing*, vol. 64, no. 5: 415-423.

Duxbury, A and A. C. Duxbury. 1994. An Introduction to the World's Oceans, 4th ed., Dubuque, IA: Wm. C. Brown Publishers, 472pp.

Eide, L. I., and S. Martin. 1975. "The formation of brine drainage features in young sea ice," *Journal of Glaciology*, vol. 14:137-154.

Eppler, D. T., L. D. Farmer, A. L. Lohanick, M. R. Anderson, D. J. Cavalieri, J. Comiso, P. Gloersen, C. Garrity, T. C. Grenfell, M. Hallikainen, J. A. Maslanik, C. Mätzler, R. A. Melloh, I. Rubinstein, and C. T. Swift. 1992. "Passive microwave signatures of sea ice," in Microwave Remote Sensing of Sea Ice. Geophysical Monograph 68, *ed.* F. Carsey. Washington, DC: American Geophysical Union, pp. 47-68

Everitt, B. 1980. Cluster Analysis. 2nd ed., New York: Halsted Press, 136pp.

Fung, A. K. and F. T. Ulaby. 1983. "Matter-energy interaction in the microwave region," in Manual of Remote Sensing, Vol. 1, *ed.* R. N. Colwell. Falls Church, VA.: American Society of Photogrammetry. pp. 115-164.

_____. 1994. Microwave Scattering and Emission Models and their Applications. Norwood, MA: Artech House, Inc., 573pp.

Garrity, C. 1991. Passive microwave remote sensing of snow covered floating ice during spring conditions in the Arctic and Antarctic. (Ph.D. dissertation, York University, CRESS department). North York, Ontario.

_____. 1992. "Characterization of snow on floating ice and case studies of brightness temperature changes during the onset of melt," in Microwave Remote Sensing of Sea Ice. Geophysical Monograph 68, *ed.* F. Carsey. Washington, DC: American Geophysical Union, pp. 313-328

_____. 1994. Microwave Scattering and Emission Models and their Applications. Norwood, MA: Artech House, Inc, 573pp.

Glen, J. W., and P. G. Paren. 1975. "The electrical properties of snow and ice," *Journal of Glaciology*, vol. 15: 15-38.

Gloersen, P., W. Nordberg, T. J. Schmugge, and T. T. Wilheit. 1973. "Microwave signatures of first-year and multiyear sea ice," *Journal of Geophysical Research,* vol. 78, no. 18: 3564-3572.

Gloersen, P., W. J. Campbell, D. J. Cavalieri, J. C. Comiso, C. L. Parkinson, and H. J. Zwally. 1992. Arctic and Antarctic Sea Ice, 1978-1987: Satellite Passive-Microwave Observations, NASA SP-511, Washington, DC: National Aeronautics and Space Administration.

Gogineni, S. P., R. K. Moore, T. C. Grenfell, D. G. Barber, S. Digby, and M. Drinkwater. 1992. "The effects of freeze-up and melt processes on microwave signatures," in Microwave Remote Sensing of Sea Ice. Geophysical Monograph 68, *ed.* F. Carsey. Washington, DC: American Geophysical Union, pp. 329-341.

Goodison, B. E., R. D. Brown, and R. G. Crane. 1999. "Cryospheric systems," in EOS Science Plan. *ed.* M. D. King. Greenbelt, MD: NASA/Goddard Space Flight Center, pp. 261-307.

Grenfell, T. C. and G. A. Maykut. 1977. "The optical properties of ice and snow in the Arctic basin," *Journal of Glaciology,* vol. 18: 445-463.

_____ and D. K. Perovich. 1984. "Spectral albedos of sea ice and incident solar irradiance in the Beaufort Sea," *Journal of Geophysical Research,* vol. 89, no. C3: 3573-3580.

_____ and A. W. Lohanick. 1985. "Temporal variations of the microwave signatures of sea ice during the late spring and early summer near Mould Bay, Northwest Territories," *Journal of Geophysical Research,* vol. 90, no. C3: 5063-5074.

_____. 1986. "Surface-based passive microwave observations of sea-ice in the Bering and Greenland Seas," *IEEE Transactions in Geoscience and Remote Sensing*, vol. GE-24, no. 3, 378-382.

_____, D. G. Barber, A. K. Fung, A. J. Gow, K. C. Jezek, E. J. Knapp, S. V. Nghiem, R. G. Onstott, D. K. Perovich, C. S. Roesler, C. T. Swift, and F. Tanis. 1998. "Evolution of electromagnetic signatures of sea ice from initial formation to the establishment of thick first-year ice," *IEEE Transactions on Geoscience and Remote Sensing*, vol. 36, no. 5:1642-1654.

Hallikainen, M. T., F. T. Ulaby, and M. Abdelrazik. 1986. "Dielectric properties of snow in the 3 to 37GHz range," *IEEE Transactions on Antennas and Propagation*, AP-34:1329-1340.

Hallikainen, M., and D. P. Winebrenner. 1992. "The physical basis for sea ice remote sensing," in Microwave Remote Sensing of Sea Ice. Geophysical Monograph 68, *ed.* F. Carsey. Washington, DC: American Geophysical Union, pp. 29-46.

Han, Y., and E. R. Westwater. 2000. "Analysis and improvement of tipping calibration for ground-based microwave radiometers," *IEEE Transactions in Geoscience and Remote Sensing*, vol. 38, no. 3: 1260 –1279.

Hanesiak, J. M., D. G. Barber, and G. M. Flato. 1999. "Role of diurnal processes in the seasonal evolution of sea ice and its snow cover," *Journal of Geophysical Research,* vol. 104, no. C6: 13,593-13,603.

Hoekstra, P., and P. Cappillino. 1971. "Dielectric properties of sea and sodium chloride ice at UHF and microwave frequencies," *Journal of Geophysical Research,* vol. 76: 4922-4931.

Hollinger, J. P., B. E. Troy, R. O. Ramseier, K. W. Asmus, M. F. Harman, and C. A. Luther. 1984. "Microwave emission from high Arctic sea ice during freeze up," *Journal of Geophysical Research*, vol. 89, no. C5:8104-8122.

Holt, B. and S. A. Digby. 1985. "Processes and imagery of first-year sea ice during melt season," Journal of Geophysical Research, vol. 90, no. C3:5045-5062.

Iacozza, J. and D. G. Barber. 1999. "An examination of the distribution of snow on sea-ice," Atmosphere-Ocean, vol. 37, no. 1: 21-51.

Intergovernmental Panel on Climate Change – Work Group I (IPCC WGI). 2001. Summary for Policy Makers – Third Assessment Report. [report on-line] Cambridge University Press, 2001, accessed 24 April 2001; available from http://www.unep.ch/ipcc/pub/spm22-01.pdf; Internet.

Intergovernmental Panel on Climate Change – Work Group II (IPCC WGII). 2001. Summary for Policy Makers – Climate Change 2001: Impacts, Adaptation and Vulnerability. [report on-line] Cambridge University Press, 2001, accessed 27 September 2001; available from http://www.unep.ch/ipcc/pub/wg2SPMfinal.pdf; Internet.

Jezek, K. C., D. K. Perovich, K. M. Golden, C. Luther, D. G. Barber, P. Gogineni, T. C. Grenfell, A. K. Jordan, C. D. Mobley, S. V. Nghiem, and R. G. Onstott. 1998. "A broad spectral, interdisciplinary investigation of the electromagnetic properties of sea ice," *IEEE Transactions in Geoscience and Remote Sensing*, vol. 36, no. 5: 1633 –1641.

Kattenburg, A. 1996. "Climate models – projections of future climate," in Climate Change 1995: The Science of Climate Change, *eds.* J. T. Houghton, L. G. Meiro Filho, B. A. Callander, N. Harris, A. Kattenburg, and K. Maskell. Cambridge, UK: Cambridge University Press, pp. 285-357.

LeDrew, E. F. 1992. "Influence of polar regions on climate variability and change," in Encyclopedia of Earth System Science. *ed.* W. A. Nierenberg. Academic Press.

Langham, E. J. 1981. "Physics and properties of snow cover." in Handbook of Snow: Principles, Processes, Management and Use, *eds.* D. M. Gray and D. H. Male. Toronto: Pergamon Press, pp. 776-787.

Livingstone, C. E., K. P. Singh, A. L. Gray. 1987a. "Seasonal and Regional Variations of Active/Passive Microwave Signatures of Sea Ice," *IEEE Transactions in Geoscience and Remote Sensing*, vol. GE-25, no. 2: 159-173.

_____., R. G. Onstott, L. D. Arsenault, A. L. Gray, and K. P. Singh. 1987b. "Microwave sea-ice signatures near the onset of melt," *IEEE Transactions in Geoscience and Remote Sensing*, vol. 25, no. 2: 174-187.

Lohanick, A. W. 1990. "Some observations of established snow cover on saline ice and their relevance to microwave remote sensing," in Sea Ice Properties and Processes. CRREL Monograph 90-1. Hanover, NH: Cold Regions Research and Laboratory, 61-67.

Lomax, A. S., D. Lubin, and R. H. Whritner. 1995. "The potential for interpreting total and multiyear ice concentrations in SSM/I 85.5 GHz imagery," *Remote Sensing of the Environment*, vol. 54:13-26

Lublin, D., Garrity, C., Ramseier, R. O., and Whritner, R. 1997. "Total sea ice concentration retrieval from the SSM/I 85.5 GHz channels during the Arctic summer," *Remote Sensing of the Environment* 62: 63-76

Manly, B. F. J. 1994. Multivariate Statistical Methods – A Primer, 2nd. ed., London: Chapman and Hall, 215pp.

Mätzler, C., E. Schanda, and W. Good. 1982. "Towards the definition of the optimum sensor specifications for microwave remote sensing of snow," *IEEE Transactions in Geoscience and Remote Sensing*, vol. GE-20: 57-66.

Maykut, G. A. 1978. "Energy exchange over young sea ice in the central Arctic," *Journal of Geophysical Research*, vol. 83, no. C7, 3646-3658.

_____. 1986. "The surface heat and mass balance" in The Geophysics of Sea Ice. NATO ASI Series, Series B Physics, vol 146, *ed.* N. Untersteiner. New York: Plenum, pp. 395-464

_____ and Perovich, D. K., 1987. "The role of shortwave radiation in the summer decay of a sea ice cover," *Journal of Geophysical Research,* vol. 92: 7032-7044.

Mellor, M. 1965. "Optical properties of snow," CRREL Research Report 169. 20pp.

Mundy, C. J., Papakyriakou, T. N., Harouche, I. 2000a. "Section 2.1. Meteorology," in C-ICE 2000 Field Summary. CEOSTEC-2000-12-01, *ed.* Iacozza, J. and D.G. Barber. Winnipeg, MB, pp. 33-39.

_____. 2000b. "Section 2.4. Snow physical properties," in C-ICE 2000 Field Summary. CEOSTEC-2000-12-01, *ed.* Iacozza, J. and D.G. Barber. Winnipeg, MB, pp. 33-39.

Nakamura, N., and A. H. Oort. 1988. "Atmospheric heat budget of the polar regions." *Journal of Geophysical Research*, vol. 93, no. D8, 9510-9524.

Nakawo, M. and N. K. Sinha. 1984. "A note on the brine layer spacing of first-year sea ice," *Atmosphere-Ocean*, vol. 22, no. 2: 193-206.

Neumann, G. and W. J. Pierson, Jr. 1966. Principals of Physical Oceanography, Englewood Cliffs, New Jersey: Prentice-Hall, 545 pp.

Oke, T. R. 1987. Boundary Layer Climates, London: Methuen & Co Ltd., 372pp.

Onstott, R. G., T. C. Grenfell, C. Matzler, C.A. Luther, and E. A. Svendsen. 1987. "Evolution of microwave sea ice signatures during early summer and midsummer in the marginal ice zone," *Journal of Geophysical Research,* vol. 92, no. C7: 6825-6835.

Papakyriakou, T. N. 1999. An examination of relationships among the energy balance, surface properties and climate over snow covered sea ice during the spring season. (Ph.D. dissertation, University of Waterloo). Waterloo, Ontario.

Parkinson, C. L., J. Comiso, H. J. Zwally, D. J. Cavalieri, P. Gloersen, and W. J. Campbell. 1987. Arctic Sea Ice, 1973-1976: Satellite Passive Microwave Observations, NASA Special Publication, SP-489, 295 pp.

_____ and P. Gloersen. 1993. "Global sea ice coverage" in Atlas of Satellite Observations Related to Global Change, ed. Gurney, R. J., J. L. Foster, and C. L. Parkinson. Cambridge: Cambridge University Press, 371-383

_____. 1997. Earth from Above: Using Color-Coded Satellite Images to Examine the Global Environment. Sausalito, CA: University Science Books.

_____, D.J. Cavalieri, P. Gloersen, H.J. Zwally, and J.C. Comiso. 1999. "Arctic sea ice extents, areas, and trends, 1978-1996," *Journal of Geophysical Research*, vol. 104, no. C9: 20,837-20,856.

Paterson, J. S., B. Brisco, S. Argus, and G. Jones. 1991. In-situ measurements of micro-scale surface roughness of sea ice," *Arctic*, vol 44, no. 1, Supplement 1: 140-146.

Perovich, D. K. and A. J. Gow. 1991. "A statistical description of the microstructure of young sea ice," *Journal of Geophysical Research,* vol. 96: 16,944-16,953.

_____., J. Longacre, D.G. Barber, R.A. Maffione, G.F. Cota, C.D. Mobley, A.J. Gow, R.G. Onstott, T.C. Grenfell, W.S. Pegau, M. Landry, and C.S. Roesler. 1998. "Field observations of electromagnetic properties of first-year sea ice," *IEEE Transactions on Geoscience and Remote Sensing*, vol. 36, no. 5: 1705-1715.

Rothrock, D. A., and D. R. Thomas. 1990. "The Arctic Ocean multiyear ice balance," *Annals of Glaciology*, no. 14: 252-255.

Stander, E. and B. Michel. 1989. "The effects of fluid flow on the development of preferred orientations in sea ice: laboratory experiments," *Cold Regions Science and Technology*, no. 17: 153-161.

Swift, C. T., K. St. Germain, K. C. Jezek, S. P. Gogineni, A. J. Gow, D. K. Perovich, T. C. Grenfell, and R. G. Onstott. 1992. "Laboratory investigations of the electromagnetic properties of artificial sea ice," in Microwave Remote Sensing of Sea Ice. Geophysical Monograph 68, *ed.* F. Carsey. Washington, DC: American Geophysical Union, pp. 177-200.

Tjuatja, S., A. K. Fung, and M. S. Dawson. 1993. "An analysis of scattering and emission from sea ice," *Remote Sensing Reviews*, vol. 7:83-106.

Troy, B. E., J. P. Hollinger, R. M. Lerner, and M. M. Wisler. 1981. "Measurements of the microwave properties of sea ice at 90 GHz and lower frequency," *Journal of Geophysical Research*, vol. 86: 4283-4289.

Tucker, W. B., III, T. C. Grenfell, R. G. Onstott, D. K. Perovich, A. J. Gow, R. A. Shuchman, and L. L. Sutherland. 1991. "Microwave and physical properties of sea ice in the winter marginal ice zone," *Journal of Geophysical Research*, vol. 96:4573-4587.

_____, D. K. Perovich, A. J. Gow, W. F. Weeks, and M. R. Drinkwater. 1992. "Physical properties of sea ice relevant to remote sensing" in Microwave Remote Sensing of Sea Ice. Geophysical Monograph 68, *ed.* F. Carsey. Washington, DC: American Geophysical Union, pp. 9-26

Ulaby, F. T., and K. R. Carver. 1983. "Passive microwave radiometry" in Manual of Remote Sensing, Vol. 1, *ed.* Colwell, R. N. Falls Church, VA: American Society of Photogrammetry, pp. 475-516.

_____, R. K. Moore, and A. K. Fung. 1986a. Microwave Remote Sensing: Fundamentals and Radiometry, Vol. I, Norwood, MA: Artech House, 456pp.

_____. 1986b. Microwave Remote Sensing: Radar Remote Sensing and Surface Scattering and Emission Theory, Vol. II, Norwood, MA: Artech House, 456pp.

Vant, M. R., R. O. Ramseier and V. Makios. 1978. "The complex-dielectric constant of sea ice at frequencies in the range 0.1-40 GHz," *Journal of Applied Physics*, vol. 49, no. 3: 1264-1280.

Vinnikov, K. Y., A. Robock, R. J. Stouffer, J. E. Walsh, C. L. Parkinson, D. J. Cavalieri, J. F. B. Mitchell, D. Garrett, and V. F. Zakharov. 1999. "Global warming and northern hemisphere sea ice extent," *Science*, vol. 286: 1934-1937.

Weeks, W. F. and S. F. Ackley. 1986. "The growth, structure, and properties of sea ice," in The Geophysics of Sea Ice. NATO ASI Series B: Physics vol. 146, *ed.* N. Untersteiner. New York: Plenum Press, pp. 9-164

Winebrenner, D. P., J. Bredow, A. K. Fung, M. R. Drinkwater, S. Nghiem, A. J. Gow, D. K. Perovich, T. C. Grenfell, H. C. Han, J. A. Kong, J. K. Lee, S. Mudaliar, R. G. Onstott, L. Tsang, and R. D. West. 1992. "Microwave sea ice signature modeling" in Microwave Remote Sensing of Sea Ice. Geophysical Monograph 68, *ed.* F. Carsey. Washington, DC: American Geophysical Union, pp. 137-175.

World Meteorological Organization (WMO). 1970. WMO Sea Ice Nomenclature , Terminology Codes and Illustrated Glossary, WMO/OMM/BMO 259, TP 145. Geneva.

Yackel, J. J., D. G. Barber, and J. M. Hanesiak. 2000a. "Melt ponds on sea ice in the Canadian Archipelago: 1. Variability in morphological and radiative properties," *Journal of Geophysical Research*, vol. 105, no. C9: 22,049-22,060.

_____ and D. G. Barber. 2000b. "Melt ponds on sea ice in the Canadian Archipelago: 2. On the use of RADARSAT-1 synthetic aperture radar for geophysical inversion," *Journal of Geophysical Research*, vol. 105, no. C9: 22,061-22,070.

Yackel, J. J. 2001. On the use of synthetic aperture radar (SAR) for estimating the thermodynamic evolution of snow covered first year sea ice. (Ph.D. dissertation, University of Manitoba). Winnipeg, Manitoba.

Zhang, T., K. Stamnes, and S. A. Bowling. 1996. "Impact of clouds on surface radiative fluxes and snowmelt in the Arctic and Subarctic," *Journal of Climate*, no. 9: 2110-2123.

Appendices

Appendix A: Julian Day Calendar

April

S	M	T	W	Th	F	Sa
						1 92
2 93	3 94	4 95	5 96	6 97	7 98	8 99
9 100	10 101	11 102	12 103	13 104	14 105	15 106
16 107	17 108	18 109	19 110	20 111	21 112	22 113
23 114	24 115	25 116	26 117	27 118	28 119	29 120
30 121						

May

S	M	T	W	Th	F	Sa
	1 122	2 123	3 124	4 125	5 126	6 127
7 128	8 129	9 130	10 131	11 132	12 133	13 134
14 135	15 136	16 137	17 138	18 139	19 140	20 141
21 142	22 143	23 144	24 145	25 146	26 147	27 148
28 149	29 150	30 151	31 152			

June

S	M	T	W	Th	F	Sa
				1 153	2 154	3 155
4 156	5 157	6 158	7 159	8 160	9 161	10 162
11 163	12 164	13 165	14 166	15 167	16 168	17 169
18 170	19 171	20 172	21 173	22 174	23 175	24 176
25 177	26 178	27 179	28 180	29 181	30 182	

July

S	M	T	W	Th	F	Sa
						1 183
2 184	3 185	4 186	5 187	6 188	7 189	8 190
9 191	10 192	11 193	12 194	13 195	14 196	15 197
16 198	17 199	18 200	19 201	20 202	21 203	22 204
23 205	24 206	25 207	26 208	27 209	28 210	29 211
30 212						

Appendix B: Acronyms and Abbreviations

C-ICE	**Collaborative-Interdisciplinary Cryospheric Experiment**
DMSP	**United States Defense Meteorological Satellite Program (DMSP)**
FYI	**First-year ice**
GCM	**General circulation models**
MYI	**Multiyear ice**
NASA	**National Aeronautics Space Agency**
SBR	**Surface-Based Radiometer**
SSM/I	**Special Sensor Microwave/Imager**
SWE	**Snow water equivalence**

Appendix D: Glossary

Albedo (α): ratio of the amount of solar radiation (shortwave radiation: $K\downarrow$) reflected by a given body to the amount incident upon it.

Blackbody: a body which emits and absorbs energy at the maximum possible rate pr unit area at a given wavelength for any temperature.

Brightness Temperature (T_B): a measurement relative to a *blackbody* (ideal emitter) radiating the same amount of energy per unit area as the observed body at the wavelength under consideration.

Cryosphere: portions of the Earth's surface and subsurface where water is found in solid state, such as sea ice, lake ice, river ice, snow, glaciers, and permafrost.

Diurnal: referent to daily.

Emissivity: ration of the total radiant energy emitted per unit time per unit area of a given body at a given wavelength and specific temperature to that of a blackbody under the same conditions.

Flux: rate of flow of energy.

Latent Heat: when a given system goes through a phase change, the heat released or absorbed during the change is known as latent heat.

Appendix E: List of Symbols

α	Albedo
°C	Degrees Celsius
ε	Complex Dielectric Constant
ε'	Permittivity
ε''	Dielectric loss
e	Emissivity
GHz	Gigahertz
H	Horizontal polarization
K	Degrees Kelvin
$K\uparrow$	Upwelling shortwave radiation
$K\downarrow$	Downwelling shortwave radiation
ρ	Density
V	Vertical polarization

Appendix F: SBR Control Software Algorithm

This algorithm was used in the control software for calibration purposes. It is restated here according to information provided by the Climate and Atmospheric Research Directorate (Meteorological Service of Canada – Ice and Marine Service Branch). These equations are reproduced from e-mail correspondence from Mr. Cam Grant and Mr. Ken Asmus.

$$T_B = T_{atm}\left[1 - e^{-(\tau \sec(\theta))}\right] + 3e^{(\tau \sec(\theta))}$$

Where τ is the normal optical depth of the atm; θ is the zenith angle; T_{atm} is the effective atmospheric temperature. Since the atmosphere is optically thin, then:

$$T_B = T_{atm}[\tau \sec(\theta)] + 3[1 - \tau \sec(\theta)]]$$

defining $M = (T_{atm} - 3)\tau C$, where C is a constant, then

$$T_B = M \sec(\theta) + 3, \text{ if } \sec(\theta) = x$$

$$T_B = Mx + 3A, \text{ where } A \text{ is a straight line}$$

The voltage V is proportional to the brightness temperature T_B according to:

$$V_B = A(Mx + 3)$$

$$\boxed{V_B = Yx + B}$$